RESEARCH OF SUPER PERMEABILITY
$NiFe/SiO_2/Cu$ COMPOSITE WIRES FOR MICRO
MAGNETIC SENSORS

WU JI

(B.Eng, HUST)

A THESIS SUBMITTED

FOR THE DEGREE OF MASTER OF ENGINEERING

DEPARTMENT OF MECHANICAL ENGINEERING

NATIONAL UNIVERSITY OF SINGAPORE

2010

_____

Acknowledgements

First and foremost, I would like to express my sincere gratitude to my supervisor **Professor Li Xiaoping**. It has been an honor as his student. In the past two years, he not only offered me the valued supervision, but also provided me inspiring guidance and significant advices throughout the entire project, without which this project cannot be completed successfully.

Furthermore, I deeply appreciate **Dr. Fan Jie** and **Dr. Ning Ning** for their constructive advices and patient assistance in executing the entire project, which played important role in conducting experiments and making my Master experience productive. At the same time, the joy gained in the course of working with them was motivational for me, even during the tough time in pursuit of my Master degree.

Moreover, I am grateful to **Dr. Seet Hang Li** and **Dr. Yi Jiaobao** for their ardent assistance and technical support to the project.

Last but not least, I would like to thank the former students of Final Year Project and UROP for their important contributions to the project as well as thank the personnel from Advanced Manufacturing Laboratory (AML) and workshop 2 for their assistance in developing the experimental setups.

Table of Contents

Summary

Extremely high permeability magnetic materials play significant role as sensing elements in the application of ultra-weak magnetic field detection sensors. In order to achieve the super permeability, a variety of magnetic materials and an extensive range of structures of sensing elements have been developed in the past decade. In this thesis, the main objective will concentrate on the study of a novel magnetic sensing element, $NiFe/SiO_2/Cu$ composite wire to further enhance the permeability of magnetic sensing elements.

Three main aspects of research have been carried out in this study: the investigation of the GMI effect in the $NiFe/SiO_2/Cu$ composite wire in relation to the insulation layer SiO_2, the optimization of the insulation layer SiO_2 to achieve the improved performance of $NiFe/SiO_2/Cu$ composite wire, and the study of NiFe layer for further enhancement in the permeability of $NiFe/SiO_2/Cu$ composite wire.

First of all, it was concluded that the addition of the insulation layer is capable of enhancing the GMI effect in the $NiFe/SiO_2/Cu$ composite wire by increasing the eddy current and the impedance of NiFe layer as well as improving its magnetic properties, such as the softness and anisotropy. At the same time, the existence of the insulation layer also could influence the frequency dependence of the MI curve and a superior frequency range (2 MHz

and 10 MHz) was obtained in the $Ni_{80}Fe_{20}/SiO_2/Cu$ composite wire for micro magnetic sensor applications.

Furthermore, the investigation of optimum parameters for the insulation layer SiO_2 in the $NiFe/SiO_2/Cu$ composite wire was conducted with various thicknesses of insulation layers. It was found that the thickness of the insulation layer at the magnitude of micrometers displayed the larger GMI effect compared to the wire with the insulation thickness at the magnitude of nanometers with an optimum thickness of 5 μm. This might be due to the enhancement of the interaction between the ferromagnetic shell and the copper core by the thick insulation layer and the increase in the thickness of insulation layer could improve the circumferential permeability of the $Ni_{80}Fe_{20}/SiO_2/Cu$ composite wire. Moreover, it was observed that the thicker insulation layer could reduce the frequency of the maximum MI ratio in the $Ni_{80}Fe_{20}/SiO_2/Cu$ composite wire by enhancing the skin effect.

In addition, the investigation of the optimum thickness proportion of NiFe and SiO_2 layers and the improved current density for electroplating NiFe layer were carried out. An optimum thickness proportion of the SiO_2 and $Ni_{80}Fe_{20}$ layers, 1.2, was found, where the thickness of the insulation layer and the ferromagnetic layer were 5 and 6 μm, respectively. The result can be explained by the competition between the improvement in the magnetic properties of NiFe layer and the influence of skin effect as the increase in the thickness of NiFe layer. An optimized plating current density, 4 A/dm^2, was also found as a result of the competition between the enhancement of

circumferential permeability by the induced circumferential magnetic field and

the reduction in the permeability caused by stress induction in the NiFe layer.

List of Tables

_____

List of Figures

_____

___

List of Publications

1. J. Fan, N. Ning, J. Wu, X.P. Li, H. Chiriac, "Study of the Noise in Multicore Orthogonal Fluxgate Sensors Based on Ni-Fe/Cu Microwire Arrays", IEEE Trans. Magn., Volume 45, Issue 10, Oct. 2009, 4451-4454

2. J. Fan, J. Wu, N. Ning, X.P. Li, H. Chiriac, "Dynamic Interactive Effect in Amorphous Microwire Array", accepted by IEEE Trans. Magn.

Chapter 1

Introduction

1.1. Motivation

The study of novel types of magnetic sensing elements with extremely high sensitivity is a very hot and promising area nowadays since the micro magnetic sensors play an essential role in realms of military, industry, medicine and science by the advantage of detecting weak magnetic fields. For example, many of countries such as the USA, the UK, Singapore, and China have established the special institutions for the development of such high performance magnetic sensing elements and a huge amount of funding has been invested in this field annually.

A composite wire $Ni_{80}Fe_{20}/Cu$ drew a great of attention worldwide due to its capacity for displaying a large potential for achieving extremely high sensitivity. To date, a series of research have been conducted in terms of this sensing element, including the material composition of the magnetic shell NiFe, the nanocrystalline grain size of the coating layer, the level of residual stresses in the composite wire, et al. Some of promising results have been obtained, for example, the maximum GMI ratio of up to 1200% has been reported at frequency around 1 MHz for maximum applied fields H_{max} [1]. Until recently, scientists discovered that the performance of $Ni_{80}Fe_{20}/Cu$ could be possibly enhanced further by adding an insulation layer, such as a SiO_2 layer, in between the ferromagnetic layer $Ni_{80}Fe_{20}$ and the conductive Cu core.

It is speculated that the permeability and anisotropy of magnetic coating materials in this novel composite structure might be improved.

The new discovery aroused interests of scientists from all parts of world immediately, there has been, however, virtually non-existent systematic scientific research on magnetic properties and sensing performance of NiFe/insulation layer/Cu composite wire yet, despite its potential scientific impact. Therefore, this challenge leads to the motivation behind this project of studying the magnetic properties and the sensing performance of NiFe/SiO_2/Cu composite wire to achieve super permeability for the micro magnetic sensor use.

1.2. Objectives

The main objective of this project is to research on magnetic properties of NiFe/SiO_2/Cu composite wire, focusing on the study of the GMI effect of the NiFe/SiO_2/Cu composite wire, the investigation of optimum parameters for the insulation layer, and the optimization of NiFe layer in the NiFe/SiO_2/Cu composite wire, as detailed below:

1. To study the effect of insulation layer in NiFe/SiO_2/Cu composite wire on the GMI response , in comparison with the $Ni_{80}Fe_{20}$/Cu composite wire;

2. To research on parameters of the insulation layer to achieve improved magnetic properties and sensing performance of NiFe/SiO_2/Cu composite wire;

3. To optimize the ferromagnetic NiFe layer in terms of the thickness proportion of the SiO_2 and the NiFe layer and the electroplating current

_____

density to enhance the sensing performance of NiFe/SiO$_2$/Cu composite wire further.

1.3. Organization of Thesis

In this thesis, the background of this project in relation to the importance of micro magnetic sensors and magnetic sensing elements is presented in *chapter 1*, in which the project objectives are also given. In *Chapter 2*, the existing types of micro magnetic sensors and sensing elements are stated. At the same time, *Chapter 2* reviews the relevant magnetic materials and significant magnetic theories, as well as the electrodeposition method used in this project. *Chapter 3* describes the proposed research approach and various fabrication and characterization setups used in this study. *Chapter 4* presents the study of the GMI effect on magnetic properties of NiFe/SiO$_2$/Cu composite wire in relation to the addition of the insulation layer. *Chapter 5* describes the investigation of the optimum parameters of insulation layer in NiFe/SiO$_2$/Cu composite wire. The optimization of ferromagnetic NiFe layer in NiFe/SiO$_2$/Cu composite wire is presented in *Chapter 6*. In the end, conclusions of this project are drawn in *Chapter 7* and recommendations are also given in this chapter.

Chapter 2

Literature Review

2.1. Implications of Micro Magnetic Sensors

Micro magnetic sensors have been widely applied in a range of areas such as industry, medicine, military and space research due to its advantages of high sensitivity and low cost. For example, the ubiquitous applications can be seen from the computer disk head to the biological displacement detection, from the military sensors to the magnetic field research. Here, the main applications of micro magnetic sensors are briefly described below.

1. Industrial applications

To date, a number of industrial processes require monitoring the presence or passage of moving objects, such as the target detection, the process control, noncontact remote location, and non-destructive crack detection. Micro magnetic sensors can well fulfill the above requirements by observing the movement of the objects and responding the decrease as voltage [2]. Take the non-destructive detection of cracked regions as an example. By deploying this type of sensor, the discontinuity of the target material will produce a disturbance in the magnetic field response; furthermore, the magnitude of the disturbance is capable of identifying the size and the shape of the cracks to determine the properties of the target material.

_____

2. Biological and medical applications

Micro magnetic sensor is the most promising type of sensor to be applied in the fields of biology and medical because of its high sensitivity to detecting very weak magnetic fields. In general, biological applications require the detection range between 10^{-10}-10^{5} Oe, which can be realized by micro magnetic sensors with the sensitivity as small as 10^{-8} Oe [3]. For instance, a magnetic tracker has been used to determine the position of medical tool inside the body and to observe biomechanical motions; a magnetic moment have been able to assist people in detecting ferromagnetic dust deposited in human lung after magnetization [4]. Moreover, scientists have been focusing on developing micro magnetic sensors to detect diminution of the direction threshold of pathogens and other targeted bimolecular such as DNA, RNA and antibodies [5].

3. Magnetic anomaly detection and space research

A heavily researched type of magnetic sensors with high sensitivity is magnetic anomaly detection (MAD), involving detecting at some distance away a ferromagnetic object (e.g. ship, tank or aircraft) [6]. The sensing element as small as 1 mm in this senor can be used to detect magnetic anomaly and localized weak magnetic fields, fulfilling the detection of the Earth's magnetic fields that varies from 10^{10} to 10^{-4} Oe from the core to the crust [7]. The detection and orientation of the Earth's magnetic field have displayed promising results by employing this significant sensor. In addition, micro magnetic sensors exert essential effort on the fields of space research and aerospace applications, such as the measurement of the ambient magnetic

_____

field vector, its orientation in space, and the precise determination of the gear-tooth position in aircraft engines [8].

2.2. Overview of Existing Types of Magnetic Sensors

A wide range of micro magnetic sensors has been developed on basis of physics and material science. The working principle of main types of current micro magnetic sensors will be briefly introduced in the following.

1. Magnetic field sensors

High sensitivity is the most important advantage of this type of magnetic sensor, the sensitivity of this typical micro magnetic sensor can reach a value as high as 500%/Oe that is 500 times than that of conventional GMR sensors [8]. The operation of this type of senor is based on the phenomenon that the impedance of amorphous wires, ribbons and nanocrystalline materials decreases sharply in fields less than 50 Oe on account of skin depth effect to measure or track the presence of both of homogeneous and homogeneous magnetic fields [9]. Currently, a novel type of sensing elements $Ni_{80}Fe_{20}/SiO_2/Cu$ composite wire has been discovered to have the great potential to achieve super sensitivity.

2. Fluxgate sensors

The fluxgate magnetometer, consisting of a ferromagnetic material wound with two coils, a drive and a sense coil, have the advantage of measuring direct current fields precisely [10-11], the aircraft compass system is a representative example of the application of fluxgate magnetometers. The

_____

principal of fluxgate magnetometer is to exploit magnetic induction together with the fact that all ferromagnetic materials become saturated at high fields. The shape of the hysteresis curve is the critical factor in determining the sensitivity of fluxgate magnetometers since the change of sensing elements into and out of the situation status could be as the signal to be detected.

3. Passive, wireless magnetic sensors

These sensors are designed by combining a magnetic field sensor and the surface acoustic wave (SAW) transponder devices for measuring magnetic fields, which can yield a sufficient effect for the radio request readout by turning the resonance for one octave in the frequency domain when applied in a magnetic field [12-13]. The main advantage of this sensor is that it can be used in a magnetic field where physical contact or a wired power supply is not available. The advantages of low power consumption and small dimension also warrant their wide applications in both of defenses and industries.

4. Current sensors

The noncontact and non-coil dc/ac measurements can be realized by current sensors. Current sensors can accurately measure both dc and ac current, which flows through a nonmagnetic wire and introduces the magnetic field. Using a magnetic ring as the sensing element such as an amorphous wire or a composite wire to circulate around the nonmagnetic wires leads to measuring the impedance responses [14]. The reduced size and high sensitivity are the salient merits of this type of sensor.

_____

5. Stress sensors

Altering response with mechanical stress provides potential for developing stress and strain sensors [15]. Scientists have developed a series of stress sensors using Co-based amorphous ribbons, Co-Mn-Si-B amorphous micro-wires, Co-Fe-Si-B amorphous wires, etc. [16-17]. Their high sensitivity to a small mechanical load is very promising for practical applications.

2.3. Overview of Different Types of Magnetic Sensing Elements

The sensing element is one of the most important parts in micro magnetic sensors, properties of which directly determine the performance of sensors in terms of sensitivity, resolution and the range of sensing [18-20]. Hence, immense scientific interests have been focused on the study of such sensing elements. To date, research efforts have studied two main types of sensing elements: (1) amorphous wires and ribbons; (2) composite wires and films (Fig. 1).
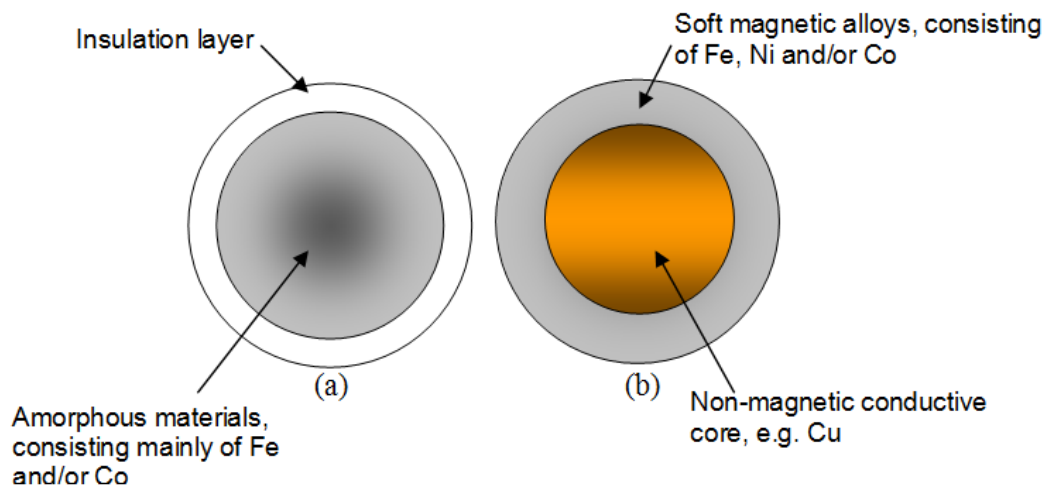
Fig. 1 (a) an amorphous wire; (b) a nanocrystalline composite wire

2.3.1. Amorphous Wires

Amorphous wires consist of mainly Fe and/or Co (70%-80%), metalloids and small amount of Cr, Al, Cu or other elements. A series of research have been conducted in the development of amorphous wires and in the study of properties of amorphous wires in the past decades [21-22]. For example, scientists have been able to fabricate amorphous wires by a range of techniques such as the quenching method, the drawing technique, or a combination of two techniques [23-28]. Furthermore, it also have been concluded that rapid quenching techniques for fabrication of amorphous wires lead to large rather frozen-in stress within the wires, which gives rise to a complex distribution of internal stresses and a core-shell structure emerges in relation to the performance of amorphous wires [24]. Therefore, some of techniques have been employed to develop improved performance, such as joule heating method, furnace-annealing method, or stress annealing method [29-32].

Furthermore, the magnetic properties of amorphous wires have been also systematically studied in terms of the composition of amorphous wires, magnetic properties measurements, etc. [33-35]. To date, a number of promising results have been reported. For instance, the maximum MI ratio of 600% at 1MHz ac testing current was achieved for $Co_{68.1}Fe_{4.4}Si_{12.5}B_{15}$ amorphous wires [36].

_____

2.3.2. Nanocrystalline Composite Wires

Nanocrystalline composite wires have also drawn a great of attention worldwide since the improved magnetic properties were discovered by producing a ferromagnetic coating layer onto a nonmagnetic rod to influence the circumference magnetic anisotropy of magnetic materials. In the meantime, the low cost of nanocrystalline composite wires is also an incentive in motivating the development of this type of sensing elements.

To date, many of fabrication processes such as electrodeposition, cold draw, and sputtering have been employed to develop nanocrystalline composite wires [37-40]. Moreover, an array of experimental studies has been carried out to optimize the performance of nanocrystalline composite wires. For example, the composition of coating permalloy, the influence of grain size of coating layers on the magnetic properties of nanocrystalline composite wires, the study of internal stresses of nanocrystalline composite wires have been well studied, which lays a solid foundation for the further research [41-42]. Particularly, a MI ratio of 1200% has been achieved for $Fe_{20}Ni_{64}Co_{16}/Cu_{97}Be_3$ microwires at ac testing current frequency of 4 MHz, while a MI% ratio of 800%-900% has been achieved for $Ni_{69}.4Fe_{22.4}Mo_{8.2}/Cu$ microwires at ac testing current frequency of 2 MHz [43].

Currently, immerse research interests have been concentrated on a novel type of glass-coated composite wire, $NiFe/SiO_2/Cu$, which exhibits great potential to enhance the permeability of the nanocrystalline composite wire so as to improve the sensing performance of micro magnetic sensors. Nevertheless, a

---

substantial amount of work still requires to be accomplished with respect to the properties and performance of this novel composite wire.

(a)

(b)
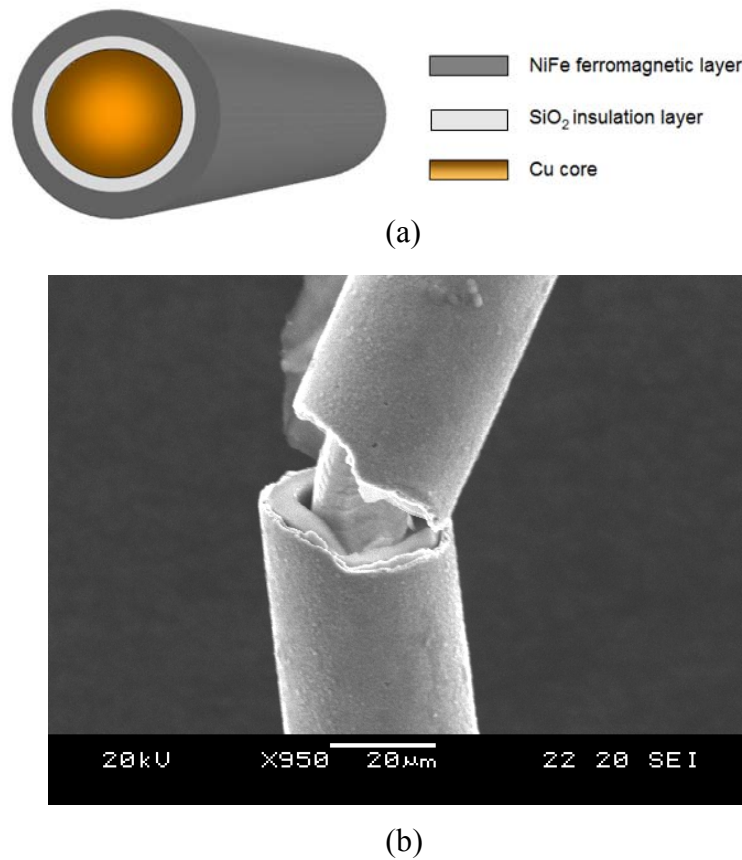
Fig. 2 (a) schematic diagram of NiFe/SiO$_2$/Cu composite wire; (b) SEM view of the cross-section of a NiFe/SiO$_2$/Cu composite wire;

2.4. Magnetic Materials

2.4.1. Ferromagnetic Materials

Ferromagnetic materials have a large, positive susceptibility to an external magnetic field, exhibiting a strong attraction to magnetic fields and being able to retain their magnetic properties after the external field has been removed. Their strong magnetic properties are correlated with the presence of magnetic domains.

Iron, nickel, and cobalt are typical examples of ferromagnetic materials. Permalloy, termed as a nanocrystalline magnetic alloy with a composition of 20% iron and 80% nickel, is a ferromagnetic material used widely as sensing elements in micro magnetic sensors because of its superior magnetic properties, such as high initial permeability, extremely low coercivity and near-zero negative magnetostriction [44].

Aside from the permalloy, supermalloy composed of 79% nickel, 4-5% molybdenum, and the rest being iron [45], Mu-metal made of 75% nickel, 15% iron, copper and molybdenum [46], alcomax consisting of an alloy of iron, nickel, aluminum, cobalt and copper [47], and alnico composed primarily of alloys of aluminum, nickel, and cobalt, with the addition of iron, copper, and sometimes titanium [48] are some of well-known ferromagnetic alloys with high magnetic permeability and low coercivity.

2.4.2. Properties of Ferromagnetic Materials

2.4.2.1. Magnetic domains

Ferromagnetic materials could exhibit a long-range ordering phenomenon at the atomic level which causes the unpaired electron spins to line up parallel with each other in a region to form a net magnetic moment, which is termed as magnetic domains. In magnetic domains, large numbers of moments (10^{12} to 10^{15}) of atoms are aligned parallel. Sizes of domains range from a 0.1 millimeter to a few millimeters. When a ferromagnetic material is not unmagnitized, the domains are nearly randomly organized and the net magnetic field is zero as a whole; on the other hand, the domains will be

aligned to produce a strong magnetic field under the force of an external magnetic field and along the direction of the external magnetic field. An illustration of the domain structure in ferromagnetic materials, such as iron, is given in Fig. 3.

The unmagnified material

Externally applied magnetic fields
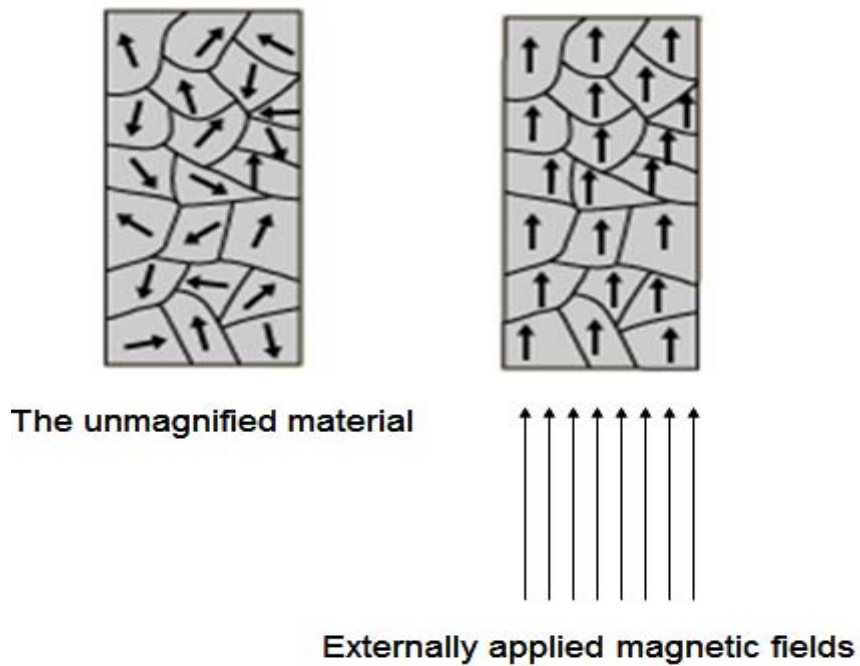
Fig. 3 the illustration of the domain structure in ferromagnetic materials

Moreover, the growth of the domains parallel to the applied field at the expense of other domains rather than the reorientation of the domains themselves could contribute more to magnetization of ferromagnetic materials in response to an external magnetic field (as shown in Fig. 4).

No external field   Weak external field   Strong external field
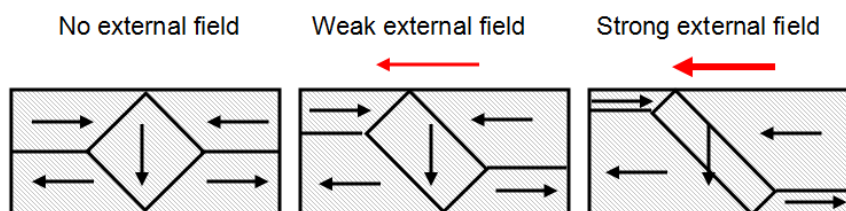
Fig. 4 the effect of external magnetic fields on magnetic domains

_____

2.4.2.2. Hysteresis

The hysteresis loop (Fig. 5) is a critical magnetic property of ferromagnetic materials, which is formed by the fact that if a ferromagnetic material is magnetized in one direction and will not return back to the original status spontaneously unless with an opposite magnetic field. In other wards, another magnetic field has to be applied in the opposite to previous one to demagnetize the materials. When the opposite is continuously being applied after the demagnetization of the ferromagnetic materials, the materials will saturate in the opposite direction, thus a loop will be traced out, namely the hysteresis loop. The hysteresis loop is closely related to the existence of magnetic domains in the materials so that a range of magnetic properties of ferromagnetic materials can be obtained in the hysteresis loop, which is briefly introduced as follow.

(1) Permeability (μ): an important magnetic property of ferromagnetic materials, describing the ease of the establishment of magnetization to evaluate the softness of materials in relation to the domain structure, the sample geometry and stress distribution in the materials and the internal configuration of magnetization. The value of permeability can be calculated by the slope of the hysteresis loop at any point.

(2) Remanence value (M_r): the remanence value is the remaining magnetization of materials in an absence of the initial driving magnetic field, which can be determined by the interception of the hysteresis loop and the magnetization axis B.

(3) Coercive force (H_c): the coercive force is the amount of reverse magnetic field to drive the magnetization to return zero.

_____

(4) Anisotropy: the anisotropy indicates the ease axis of magnetic materials and can be estimated based on the shape of the hysteresis loop. For example, if the hysteresis loop of a material appears box-shaped, which means the anisotropy of this particular material is near longitudinal; while if the shape of the hysteresis loop is curvy and round, the anisotropy is circumferential.

When the driving magnetic filed drops to zero, the ferromagnetic material remains certain degree of magnetization.

Materials magnetized to saturation by alignment of domains

The driving magnetic field must be reversed and increased to a large value to drive the magnetization to zero again.

The material follows a non-linear magnetization curve when magnetized from a zero field value

Fig. 5 a typical view of hysteresis loop (ref: http://hyperphysics.phy-astr.gsu.edu/hbase/solids/hyst.html)

2.4.3. Magneto-impedance (MI) Effect

The giant magneto-impedance (MI) effect is described as a large change in the ac impedance of a ferromagnetic material when the material is subject to a small ac alternating current. The MI ratio $\Delta Z/Z$ is usually defined as

$$\Delta Z \big/ Z = \frac{Z(H_0) - Z(H_{max})}{Z(H_{max})} (\%) \tag{1}$$

where Z is the impedance modulus and H_{max} is the maximum measuring field at which the specimen is considered to be magnetically saturated. However,

_____

although the definition of GMI ratio $\Delta Z/Z$ has been widely used for quantifying the huge attained variations of impedance, it should be well chosen in relation to the ratio of Z/R_{dc}, where R_{dc} is the DC resistance of the sample, since the definition relies on the inaccurate H_{max} and the ratio $\Delta Z/Z$ is markedly sensitive to the measuring circuit [49].

Generally, two components consist of the giant magneto-impedance, which is expressed as

$$Z = R + iX \tag{2}$$

where R is the resistance (real part) and X is the reactance (imaginary part) when subjected to a static magnetic field, H_0 [49].

Moreover, the complex impedance of a linear electronic element at the circular frequency ω is given by:

$$Z(\omega) = U_{ac} / I_{ac} = R + iX \tag{3}$$

where I_{ac} is the harmonic current with frequency ω flowing through the element and U_{ac} is the harmonic voltage of the same frequency. This equation is only applicable under some of circumstances. In the case of ferromagnetic conductors, U_{ac} is generally not proportional to I_{ac} and the materials are not a harmonic function of time (it contains higher order harmonics) [50-51].

2.5. Magnetic Materials Deposition

2.5.1. Principle of Electrodeposition

The electrodeposition is a process of coating metallic materials on a surface in an electrolyte solution using electrical current to reduce cations of a material from a solution. During the electrodeposition, the anode is supplied by a power supply with a direct current which oxidizes the metal atoms to dissolve it in the solution; at the same time, a cathode is connected to the object to be deposited. Generally, a metal ion M^{z+} will be transferred from the solution into the ionic metal lattice [52-53]. A simplified atomistic representation of this process is

$$M^{z+}(solution) \longrightarrow M^{z+}(lattice) \tag{4}$$

The cathodic deposition is composed of three main stages. The first step is called ionic migration, in which the metallic ions migrate towards the cathode by the action of the applied current. Electron transfer then will follow the ionic migration and the metallic ions enter the diffusion double layer. Eventually, the absorbed atom will incorporate in a growth point on the cathode, which is termed as incorporation.

The electrodeposition of alloys, involving a co-deposition of metals, has the same principle of electroplating the single material but exhibits superior properties than that of a single material by adjusting the percentage of the components in the deposited alloy in terms of various material properties and magnetic properties. In this study, the electrodeposition of NiFe is realized by the control of Ni and Fe deposition rate, which can rely on the chemical

composition of the respective ions in the electrolyte. The reaction equations involved are as follows [54-56]:

$$2H_2O + 2e^- \rightarrow H_2 + 2OH^- \quad (5)$$

$$M^{2+} + OH^- \rightarrow M(OH)^+ \quad (6)$$

$$M(OH)^+ \rightarrow M(OH)_{ads}^+ \quad (7)$$

$$M(OH)_{ads}^+ + 2e^- \rightarrow M + OH^- \quad (8)$$

where M represents Ni or Fe atoms.

2.5.2. Faraday's Law of Electrolysis

In the process of electrodeposition, the proportional relationship between amount of electrochemical reaction occurring at an electrode and the quantity of electric charge Q passed through an electrochemical cell is described as Faraday's law. The Faraday's law states:

$$w = Z.Q \quad (9)$$

Where w is the weight of a product of electrolysis, Z is the electrochemical equivalent, and Q is the product of the current I. Thus, if the elapsed time is t, in seconds, it can be given that:

$$Q = I.t \quad (10)$$

$$W = I.t.Q \quad (11)$$

Based on Faraday's law, Faraday constant F is given by:

$$F = N_A e = 96,487 Cmol^{-1} \quad (12)$$

where N_A is Avogadro's number (6.0225×10^{23} molecules mol^{-1}) and e is the charge of a single electron (1.6021×10^{-19} coulombs, C).

_____

Fraction of a molar (atomic) unit of reaction that corresponds to the transfer of one electron, thus the production of one gram equivalent of a product at the electrode W_{eq} can be expressed as:

$$W_{eq} = A_{wt} / n \qquad (13)$$

where A_{wt} is the atomic weight of metal deposited on the cathode, and n is the number of electrons involved in the deposition reaction. Thus,

$$Z = W_{eq} / F = A_{wt} / nF \qquad (14)$$

$$w = Z.Q = (A_{wt} / nF).Q \qquad (15)$$

2.5.3. Current Efficiency

The relationship between the number of coulombs of electricity and the sum of the number of equivalents of each reaction is correspondent when two or more reactions occur simultaneously at an electrode. Any one of the simultaneous reactions is termed as the current efficiency CE, which can be defined as the number of coulombs required for that reaction, Q_j, divided by the total number of coulombs passed, Q_{total}:

$$CE = \frac{Q_j}{Q_{total}} \qquad (16)$$

An alternative equation defining current efficiency is

$$CE = \frac{w_j}{w_{total}} \qquad (17)$$

where w_j is the weight of metal j actually deposited and w_{total} is that which would have been deposited if all the current had been used for depositing the metal j.

_____

2.5.4. Predictions of Deposit Thickness

If the volume of the deposit V and the product of the plated surface area a are determined, the deposit thickness can be calculated base on:

$$h = V / a \tag{18}$$

where h is the deposit thickness.

The volume of the deposit can be found by the weight of the deposit w and the density of the deposit d:

$$d = w / V \tag{19}$$

Thus,

$$h = \frac{V}{a} = \frac{w}{ad} \tag{20}$$

In relation to the plating time t, the formulas can be given on basis of Faraday's law:

$$h = \frac{w}{ad} = \frac{ZQ}{ad} = \frac{ZIt}{ad} cm \tag{21}$$

$$t = \frac{had}{ZI} s \tag{22}$$

_____

2.6. Summary

In order to explain the significance of objectives in this project, an overview of the implication of micro magnetic sensors was presented firstly in terms of their important applications in areas of industry, medicine, and scientific research, which was followed by the extensive review on currently existing types of micro magnetic sensors. Various magnetic sensing elements were subsequently demonstrated, which introduced the significance of sensing elements in the development of high sensitivity magnetic sensors and revealed glass-coated composite wire is a relatively novel sensing element and potentially beneficial to the high sensitivity of the magnetic sensors although non-existence work has been done with respect to the properties and performance of this type of promising composite wire.

Review on magnetic materials in terms of the introduction to ferromagnetic materials, the properties of ferromagnetic materials, such as magnetic domains, hysterias and magneto-impedance (MI) effect, lays the author a foundation on which objectives of this project are established.

In addition, the background and relevant knowledge of electrodeposition method were stated to assist the author to understand the mechanism of research approach designed and implemented in this project.

Chapter 3

Research Approach and Experimental Setups

3.1. Research Approach

In this study, three main stages are involved throughout each experiment, which are the fabrication of composite wires, the investigation of material properties of composite wires and the testing of magnetic properties of composite wires. All the characterization methods and experimental setups are described in this chapter.

First of all, the fabrication of composite wires was conducted by electrodeposition method, in which the preparation of electrolytes, the setup of the plating cell and the electrodeposition were carried out.

In the second step, material properties of composite wires were characterized. The surface roughness and coating thickness of composite wire specimens were investigated by scanning electron microscopy (SEM); the composition of coating layer was analyzed by Energy-dispersive X-ray spectroscopy (EDX); the average nanocrystalline grain size of coating layer was verified by X-ray diffraction (XRD).

Finally, magnetic properties and performance of composite wires were studied, in which the testing of hysteresis was measured by induction method and the magneto-impedance (MI) effect was tested using MI effect setup.

3.2. Materials Development and Fabrication Processes

3.2.1. Glass Coated Melt Spinning Setup

Glass Coated Melt Spinning method was employed in this project. Fig. 6 shows a schematic illustration of the glass-coated melt spinning method, in which melt contained in a glass tube was drawn rapidly to a very fine wire together with the coating glass softened by heating using a drawing machine. After the drawing operation, metallic wires were obtained by chemical dissolution of the coating glass in hydrofluoric acid. The speed of the drawing process could enable various thicknesses of glass covers to be developed. Copper wires of 20 μm in diameter with different thicknesses of SiO_2 were fabricated in this project.
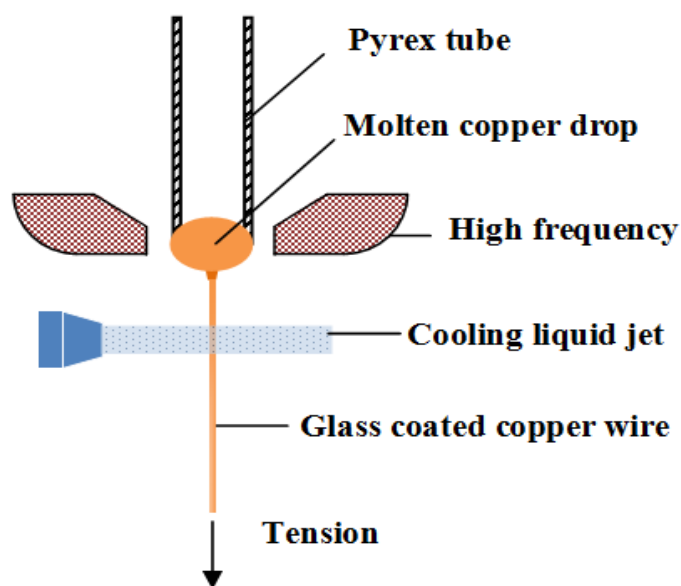
Fig. 6 schematic illustration of the glass-coated melt spinning method

3.2.2. Magnetron Sputtering Setup

In the fabrication process of the $NiFe/SiO_2/Cu$ composite wire, a conductive seed layer was developed on the insulation layer in order to coat the

ferromagnetic NiFe layer on the insulation layer SiO_2. The seed layer was sputtered by the magnetron sputtering system (Denton Discovery 80 System), which is equipped with three circular magnetron cathode guns to sputter conductive materials, such as silver, on the layer of SiO_2 in the specimen. The sputtering mode used for this project was the DC sputtering mode.
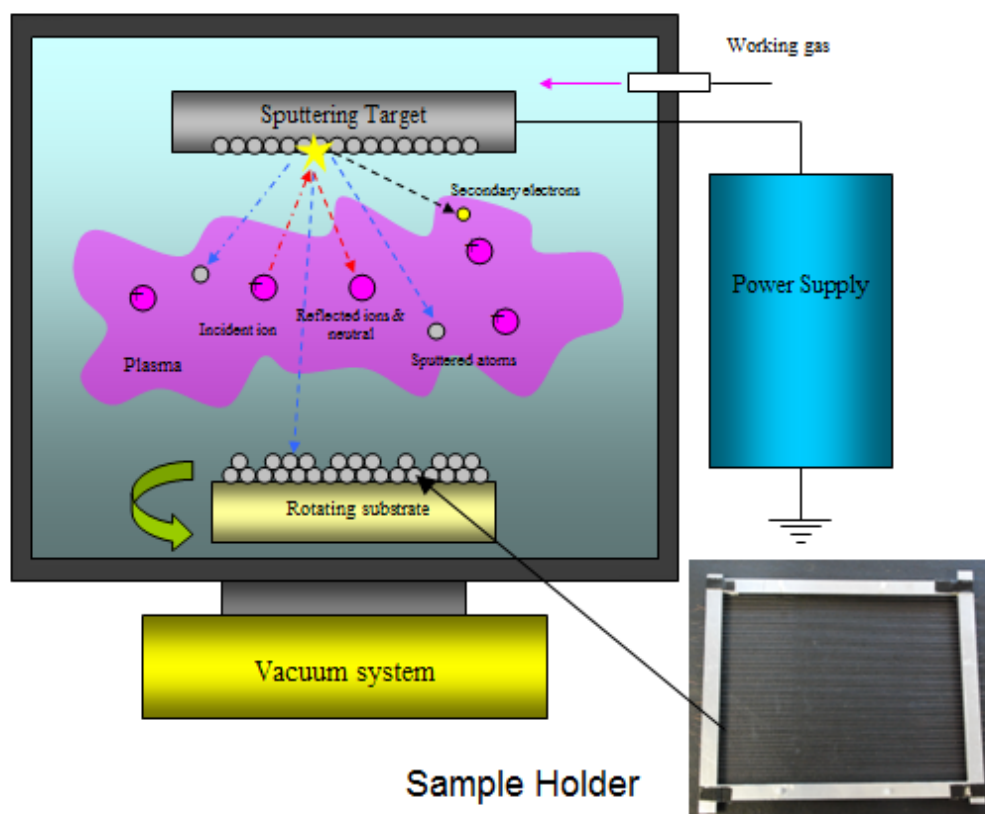
Fig. 7 schematic diagram of Denton Discovery 80 system

The glass-coated SiO_2/Cu composite wires were fixed on a sample holder (Fig. 7), the dimension of which is 200*150 mm, and then were placed into the deposition chamber. Subsequently, the vacuum pump was turned on to vacuum the chamber for the targeted condition. Sputtering deposition started after inputting the deposition parameters and satisfying the required vacuum condition. It is note that wires fixed on the sample holder only can be

sputtered on the exposed surface, the sample holder thus must be turned over and put into the chamber again for sputtering the other unexposed surface of the composite wire. This method is also applicable to sputtering the insulation layer SiO_2 on the copper wire.

Fig. 8 shows the SEM image of surface morphology of the sputtered sliver seed layer of 100 nm in thickness. It can be seen that its surface is smooth and homogenous for electrodeposition.
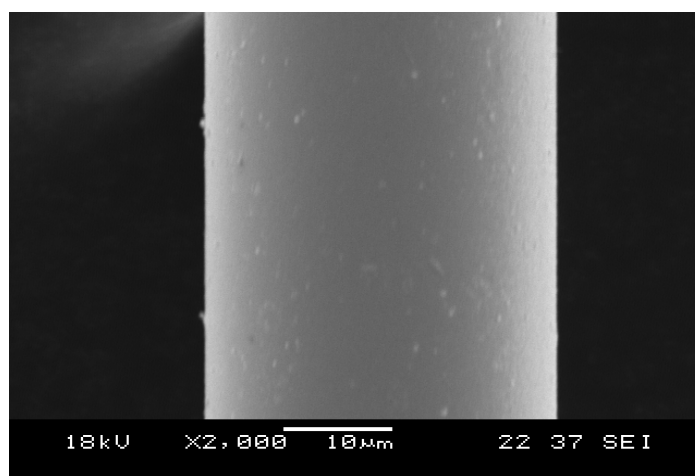
Fig. 8 SEM picture of surface morphology of the sputtered sliver seed layer

3.2.3. Chemical Electrodeposition

In this project, the electrodeposition of NiFe layers was performed in a Watts-type electrolyte solution, in which the chemical composition is as presented in Table 1.

Chemical Name / Formula	Concentration For NiFe Plating
$FeSO_4.7H_2O$	Varied
$NiSO_4.6H_2O$	125 g/L
$NiCl_2.6H_2O$	20 g/L
H_3BO_3	40 g/L
Saccharin	6 g/L

Table 1 chemical composition of electrolyte for plating the $Ni_{80}Fe_{20}$ layer

The chemicals $FeSO_4.7H_2O$ and $NiSO_4.6H_2O$ are the main sources of Fe^{2+} and Ni^{2+} ions in the electrolyte solution. The amount of $FeSO_4 \cdot 7H_2O$ is varied due to it should be accordingly adjusted at various coating thicknesses of $Ni_{80}Fe_{20}$ layers and the plating current density to obtain the required ratio of 80:20 for Ni and Fe. $NiCl_2.6H_2O$ provides Ni^{2+} and Cl^- ions for the solution. The presence of Cl^- ions in the solution improves the throwing power of the solution. Boric acid (H_3BO_3) is added to the solution as a pH buffer element, i.e. to maintain consistent pH value of the solution throughout the plating process. Saccharin is compounded in the solution as a class brightener in order to attain deposited layers of smaller average grain sizes. In this thesis, five to seven samples were produced for each wire in the experiments.

A prepared wire sample, seed layer/SiO_2/Cu, was fixed to the center of a stainless plating cell and connected to the cathode of Advantest R6243 DC Voltage Current Source; at the same time, the plating cell was connected to the anode of the current source. The electrolyte solution in a water bath was maintained at a constant temperature of 55℃. The pH value of the electrolyte solution was kept at the value of 3.4 by the addition of Potassium hydroxide

pellets (KOH). A schematic diagram of the electrodeposition process is presented in Fig. 9.
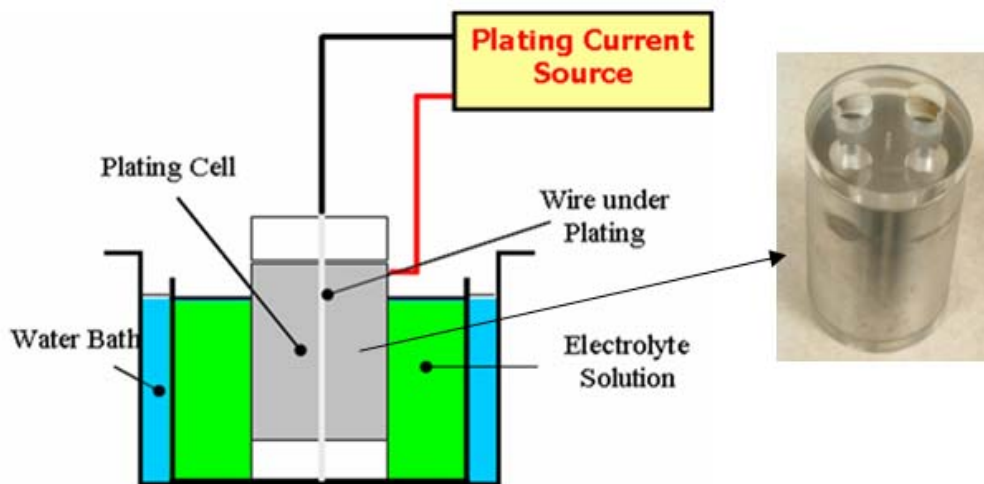
Fig. 9 schematic diagram of chemical electrodeposition setup

When the current flows through the conductive seed layer, an anomalous co-deposition of Ni-Fe on the cathode occurs as followed due to a potential difference between the plating cell and the cathode:

$$Ni^{2+} + 2e^- \rightarrow Ni \tag{23}$$

$$Fe^{2+} + 2e^- \rightarrow Fe \tag{24}$$

$$Ni^{2+} + 2OH^- \rightarrow Ni(OH)_2 \tag{25}$$

$$H_2O \rightarrow H^+ + OH^- \tag{26}$$

$$H^+ + H^+ + 2e^- \rightarrow H_2 \tag{27}$$

where Eqn. 23 and Eqn. 24 are reactions responsible for the deposition of the ferromagnetic alloy at the cathode, Eqn. 25 is the reaction causing the deposition of ferromagnetic alloy NiFe to be of an anomalous nature, and Eqn. 26 and Eqn. 26 show the reactions results in hydrogen gas evolution during electrodeposition.

3.3. Materials Properties Characterization Setup

3.3.1. Scanning Electron Microscopy (SEM)

Scanning Electron Microscopy (SEM) is a type of electron microscope with a high-energy beam of electrons in a raster scan pattern. In the working process, a beam of electrons is produced at the top of microscope by heating a metallic filament, and the electron beam follows a vertical path through the column of the microscope to pass through the electron lenses which focus and direct the beam down towards the sample. Once the electron beam hits the sample, backscattered or secondary electrons will be ejected. The detectors collect and convert electrons to a signal that will be sent to the view screen and an image is produced. The surface uniformity of the electroplated NiFe layers was examined by using SEM in this project, the thickness of NiFe layers could be calculated according to the SEM images. The schematic presentation of a scanning electron microscope is illustrated in Fig. 10.
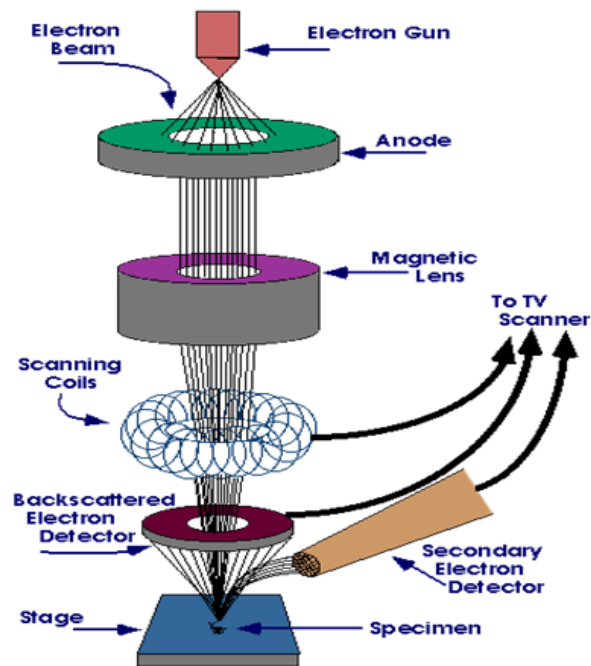
Fig. 10 schematic presentation of SEM (ref:
http://www.purdue.edu/rem/rs/sem.htm)

JEOL scanning electron microscopy (SEM) was used in this project. The magnification range of this particular SEM is from 15× to 200,000× and its resolution is 5 nanometres. Most of samples were observed at the magnification of 1500× and at the voltage of 20 kV in the experiments. A typical SEM picture of a composite wire specimen is shown in Fig. 11.
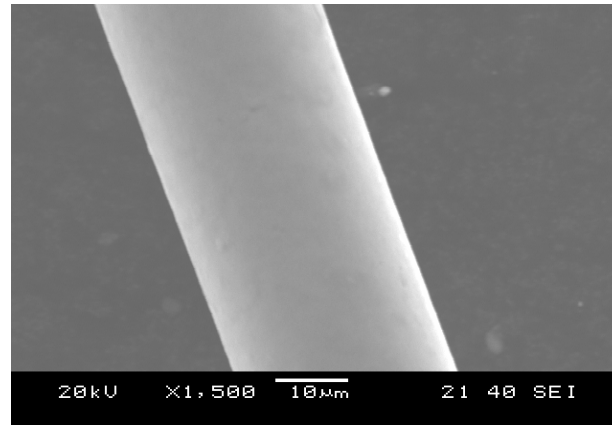
Fig. 11 a typical SEM picture of a composite wire specimen

3.3.2. Energy Dispersive X-ray (EDX)

Energy dispersive x-ray (EDX) is a chemical microanalysis technology used in conjunction with SEM. In course of the analysing the chemical composition of a specimen, an electron beam strikes the surface of the sample, where x-ray emitted will be detected to characterize the elemental composition of the analysed samples. The detector is typically a lithium device that creates a charge pulse proportional to the energy of the x-ray when an incident x-ray strikes the detector. The charge pulse will be converted to a voltage pulse and then be sent to a multichannel analyser where the pulses are sorted by voltage. The voltage measurement for each incident x-ray is sent to a computer for display and further data evaluation. Features or phases as small as 1 μm or less can be analysed. The chemical composition results of NiFe layers were

measured using EDX in this project. A typical analysis result of composite wires is shown in Table 2.

Element	(keV)	mass%	Error%	At%	Compound	mass%	Cation	K
Fe K	6.398	18.06	0.48	18.81			20.0758	
Ni K	7.471	81.94	0.95	81.19			79.9242	
Total		100.00		100.00				

Table 12 a typical EDX analysis result of a composite wire

3.3.3. X-Ray Diffraction (XRD)

X-Ray Diffraction (XRD) is a method of determining the arrangement of atoms within a crystal by using a diffracted beam, composed of a large number of scattered rays mutually reinforcing one another, strikes a crystal and diffracts into many specific directions to measure the average spacing between layers or rows of atoms, determine the orientation of a single crystal or grain, find the crystal structure of an unknown material and measure the size, shape and internal stress of small crystalline regions. The atomic planes of a crystal cause an incident beam of X-rays to interfere with one another as leaving the crystal. In materials, an electron in an alternating electromagnetic field will oscillate with the same frequency as the field. In almost all directions destructive interference will be obtained, which demonstrates that the combining waves are out of phase and there is no resultant energy leaving the solid sample. However the atoms in a crystal are arranged in a regular pattern, and in a very few directions constructive interference will be detected. The waves will be in phase and there will be well defined x-ray beams leaving the sample at various directions. Fig. 12 presents a schematic diagram of XRD.

In this project, XRD diffraction patterns were recorded using a Philips 7000 diffractometer with Cu Kα radiation. θ-2θ scans were performed at 2°min-1. For example, Fig. 13 shows measured XRD spectra of NiFe/Cu composite wire obtained by electrodeposition. The XRD spectra showed a FCC Cu layer (with lattice constant a = 0.355 nm) and also a FCC NiFe layer (with lattice constant a = 0.362 nm) on top. The ratio between these intensities can be used to calculate the amount of crystallinity in the material.
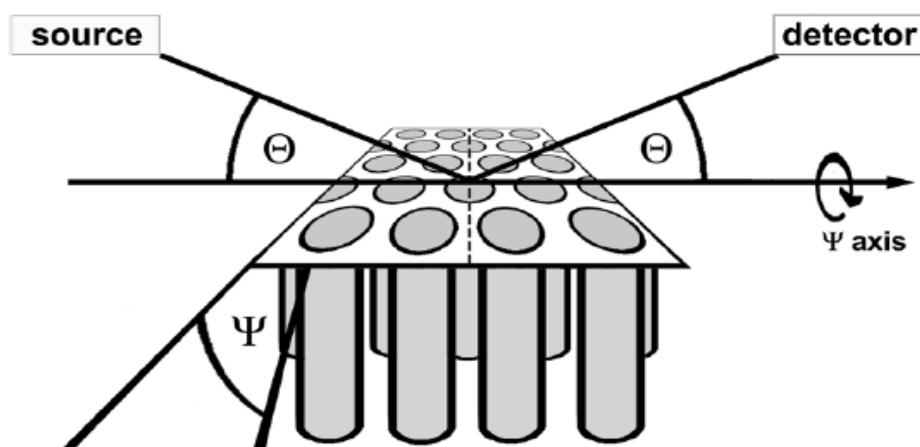
Fig. 12 schematic presentation of XRD
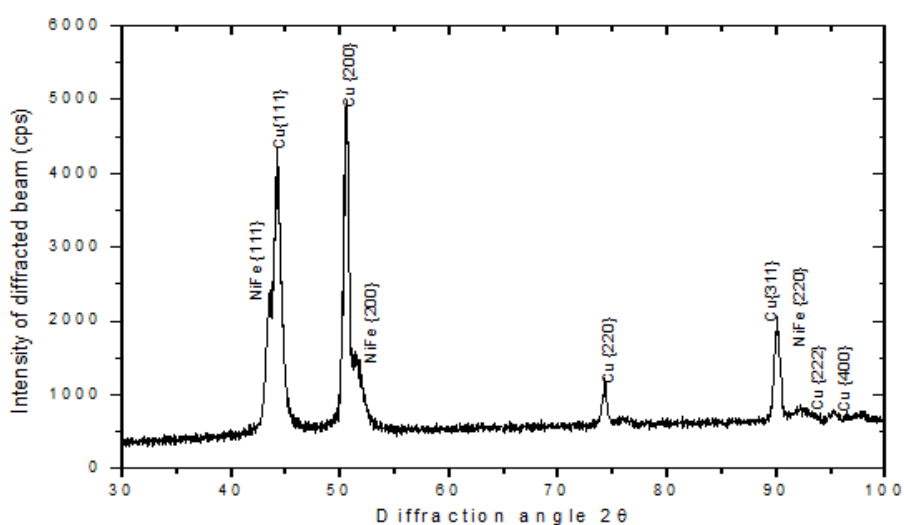
Fig. 13 XRD data of a NiFe/Cu composite wire

3.4. Magnetic Properties Characterization Setup

3.4.1. Inductance Method Setup

The hysteresis loop was measured by inductance method in this project. In this setup, a long solenoid driven by an 80 Hz triangular signal creates the magnetic axial field H. A 25-cm-long sample is placed into a 1000 turns of pick-up coil, in which a voltage will be induced by the changes in the longitudinal component of the magnetization. A second compensating coil is connected in the opposition to cancel the contribution of field H. The value of the magnetization is obtained by integration of the pick-up signal, and is plotted versus the corresponding H field. The schematic diagram of inductance method and a typical view of hysteresis loop result are illustrated in Fig. 14 and Fig. 15, respectively.
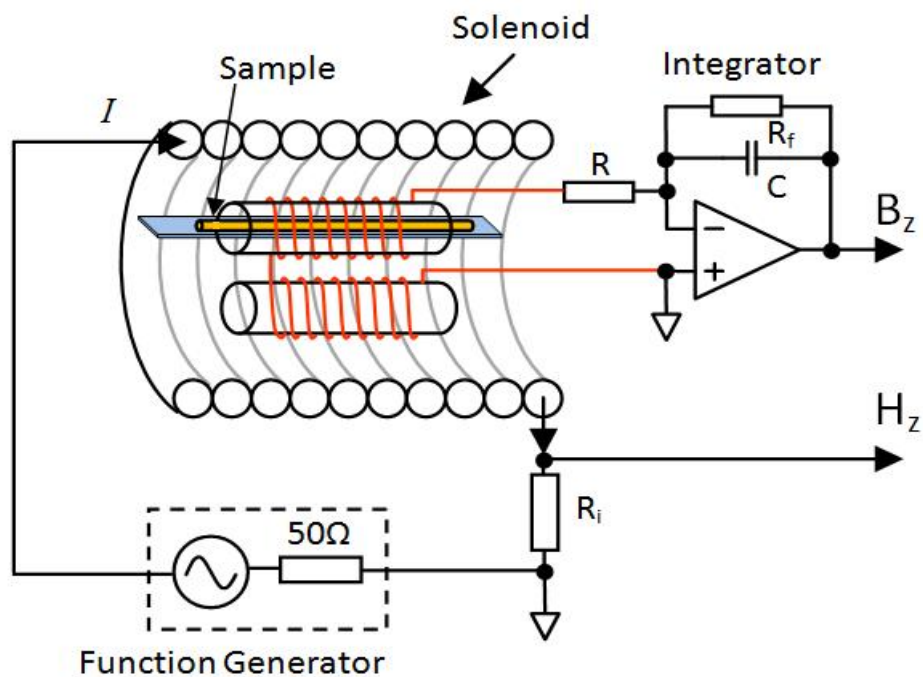
Fig. 14 schematic diagram of induction method
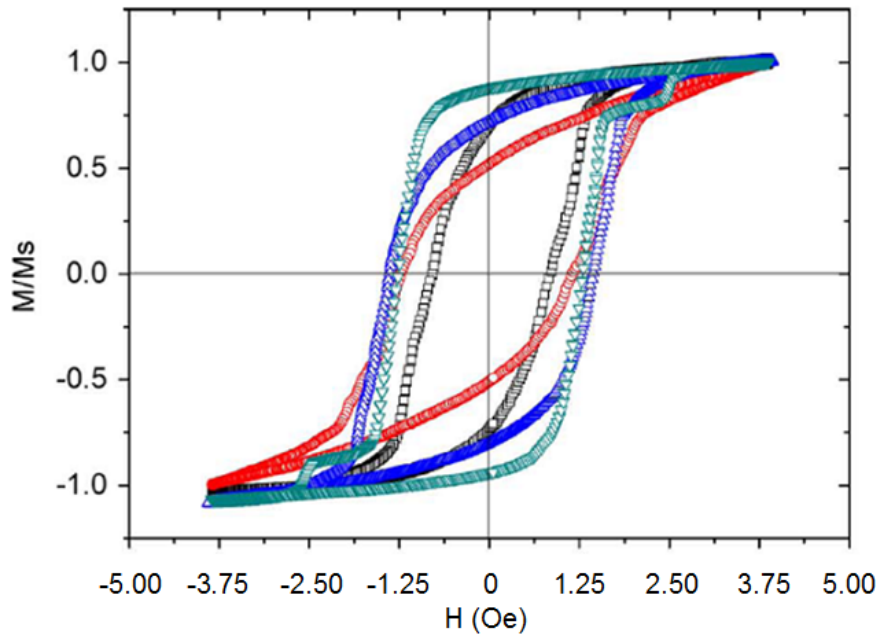
Fig. 15 a typical view of hysteresis results

3.4.2. Magneto-impedance (MI) Effect Testing Setup

Magneto-impedance (MI) testing method was employed to investigate the GMI effect of composite wires in this project. In the testing process, an ac current was passed through a composite wire sample and a circumference magnetic field around the wire was induced. The RMS value of the ac driving current was kept constant at 10 mA, and its frequency ranged from 100 kHz to 50 MHz. The magneto-impedance measurements were carried out by using a precision impedance analyzer (HP4294A).

The external magnetic fields were produced by changing the DC current through the Helmholtz coils with the range of 0.05 mA to 2.5 mA. The schematic diagram of magneto-impedance (MI) measurement is illustrated in Fig. 16.
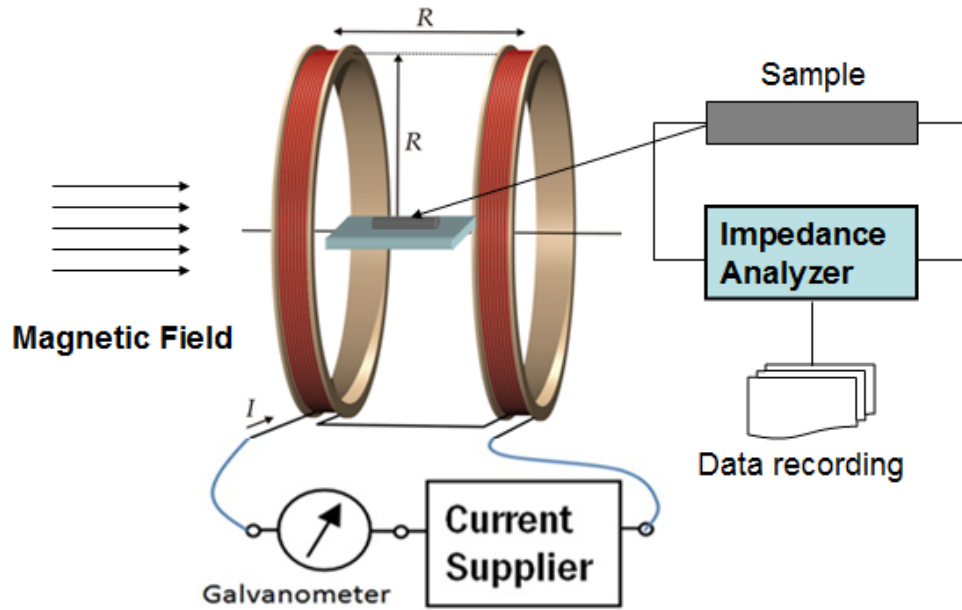
Fig. 16 schematic diagram of magnetoimpedance measurement setup

Relative change of the impedance (Z) with the applied field (H) is expressed as

$$\Delta Z \Big/ Z = \frac{Z(H_0) - Z(H_{max})}{Z(H_{max})} (\%)$$

where H_{max} is usually the external magnetic field sufficient to saturate the impedance. In practice, the value of H_{max} is available for given experimental equipment and a typical MI curve of a tested specimen composite wire is given in Fig. 17.
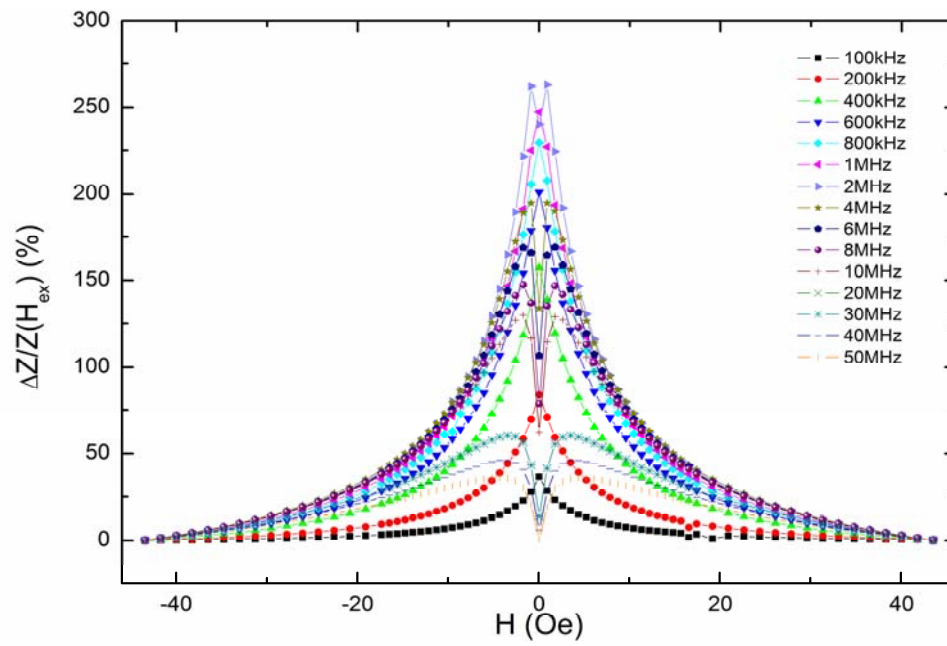
Fig. 17 typical MI curves of a composite wire

_____

Chapter 4

Research on GMI Effect in NiFe/SiO$_2$/Cu Composite Wire in relation to Insulation Layer SiO$_2$

In order to investigate the insulation layer effect on the magnetic properties and sensing performance of NiFe/SiO$_2$/Cu composite wire, the specimens of Ni$_{80}$Fe$_{20}$/SiO$_2$/Cu and Ni$_{80}$Fe$_{20}$/Cu composite wires were fabricated in this study with the same composition and thickness of NiFe layer. Specifically, the same electrolyte and the equal electroplating current density (2 A/dm^2) were employed to guarantee the composition of Ni$_{80}$Fe$_{20}$ layer; the thickness of Ni$_{80}$Fe$_{20}$ layer was controlled by the manipulation of plating duration based on following formulas:

$$T = -\frac{2}{30}J + \frac{670}{3} \qquad (28)$$

$$J = \frac{I}{2\pi rl} \qquad (29)$$

Where l and r are the length and radius of the deposited wire respectively; J is the current density in the process of electrodeposition; I is the strength of the current flowing through the wire; and T is the plating duration required to control the thickness of the NiFe layer.

Fig. 18 shows the SEM image of surface morphology of electroplated Ni$_{80}$Fe$_{20}$/SiO$_2$/Cu composite wire. It can be seen that the surface of Ni$_{80}$Fe$_{20}$ layer is smooth and homogenous. In this experiment, the thickness of SiO$_2$

_____

insulation layer and the diameter of Cu core are 3 μm and 20 μm, respectively.

Hence, the calculated thickness of Ni$_{80}$Fe$_{20}$ layer in Fig. 18 is 1.5 μm.
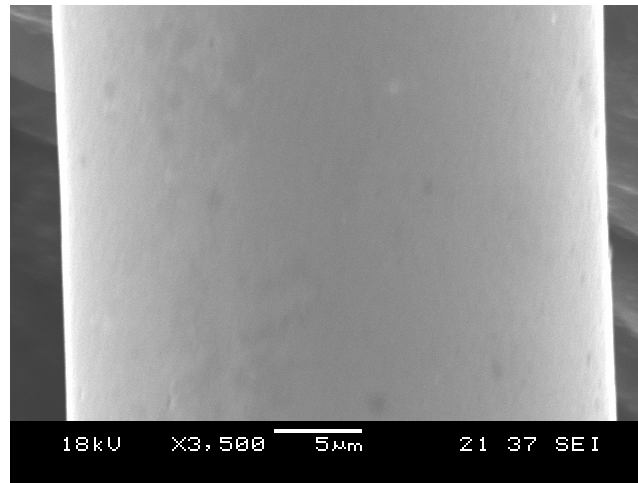
Fig. 18 SEM view of the surface morphology of electroplated Ni$_{80}$Fe$_{20}$ layer

Since the potential of insulation layer in Ni$_{80}$Fe$_{20}$/SiO$_2$/Cu composite wire for

the enhancement of GMI effect is based on its role in isolating the conductive

Cu core and the ferromagnetic NiFe layer, the ac driving current only flowed

through the Cu core in the process of testing GMI effect in Ni$_{80}$Fe$_{20}$/SiO$_2$/Cu

composite wire (Fig. 19); while the Cu core and the ferromagnetic NiFe layer

were both connected to the ac driving current in Ni$_{80}$Fe$_{20}$/Cu composite wire.
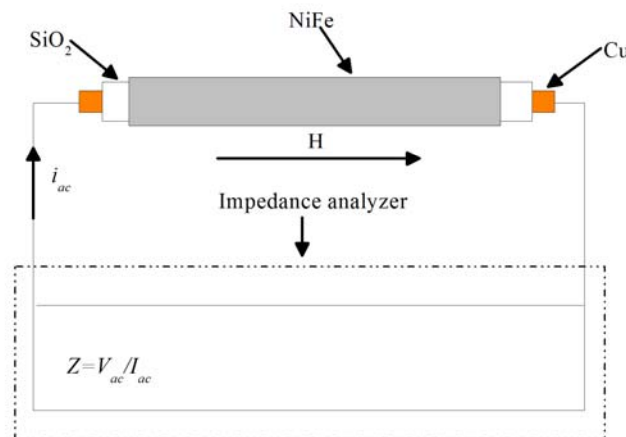
Fig. 19 schematic diagram of MI testing for the Ni$_{80}$Fe$_{20}$/SiO$_2$/Cu composite
wire

4.1. GMI Effect in NiFe/SiO$_2$/Cu Composite Wire

Fig. 20 (a) and (b) display the field dependence of MI ratios of the Ni$_{80}$Fe$_{20}$/SiO$_2$/Cu and the Ni$_{80}$Fe$_{20}$/Cu composite wires at various frequencies from 100 kHz to 500 MHz, the ac driving current was fixed at 10 mA.
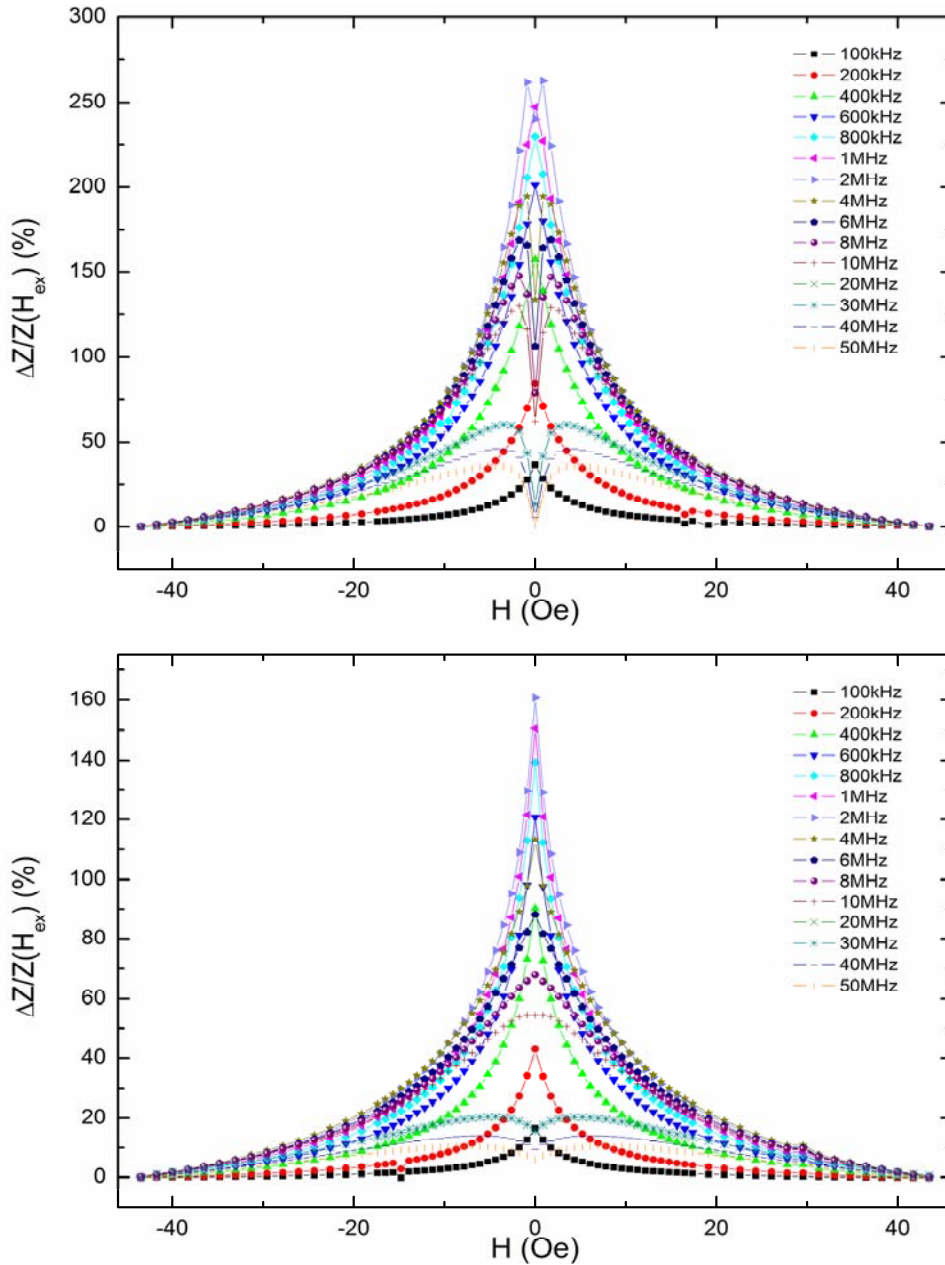
Fig. 20 field dependence of MI ratios of the Ni$_{80}$Fe$_{20}$/SiO$_2$/Cu composite wire (a) and the Ni$_{80}$Fe$_{20}$/Cu composite wire (b), tested at frequencies from 100 kHz to 500 MHz

_____

It can be seen in Fig. 21 that the maximum MI ratio of 262.75% was obtained

in the Ni$_{80}$Fe$_{20}$/SiO$_2$/Cu composite wire in comparison with that of 160.68%

achieved in the Ni$_{80}$Fe$_{20}$/Cu composite wire under the same experimental

conditions, the difference between the maximum MI ratios of two types of

composite wires is 102.07%. The large enhancement of GMI effect in the

Ni$_{80}$Fe$_{20}$/SiO$_2$/Cu composite wire can be attributed to two main factors, both of

which are closely related to the adding of the insulation layer.
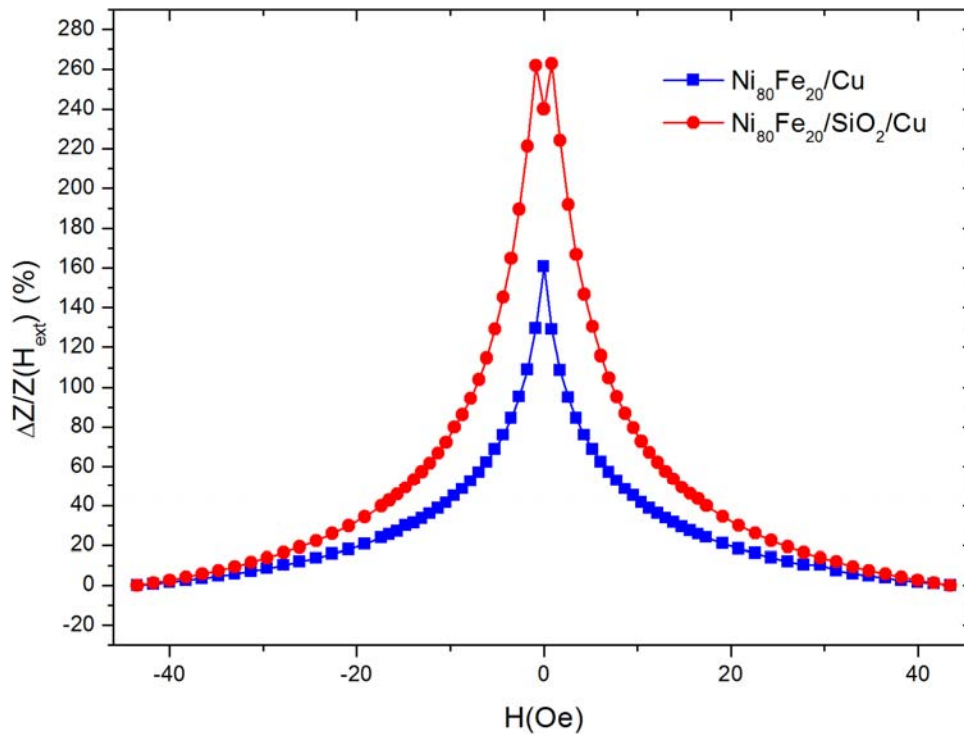
Fig. 21 field dependence of the maximum MI ratios of the Ni$_{80}$Fe$_{20}$/SiO$_2$/Cu
and the Ni$_{80}$Fe$_{20}$/Cu composite wire at 2 MHz

The first factor leading to the soar of GMI effect in the Ni$_{80}$Fe$_{20}$/SiO$_2$/Cu

composite wire is that the existence of insulation layer significantly affects the

eddy current distribution and the impedance in the Ni$_{80}$Fe$_{20}$ layer. Due to the

ac driving electric field $e=e_0exp(-i\omega t)$ is non-zero only in the core region and

the external dc magnetic field H_e is parallel to the wire axis in the testing of

_____

GMI effect of the Ni$_{80}$Fe$_{20}$/SiO$_2$/Cu composite wire, the distribution of magnetic fields within the conductive Cu core can be determined by the driving and eddy currents based on Maxwell equations as follows [57]:

$$e_z^{(1)}(\rho) = AJ_0(k\rho) \tag{30}$$

$$h_\varphi^{(1)}(\rho) = (4\pi\sigma_1/ck)AJ_0(k\rho) \tag{31}$$

$$e_\varphi^{(1)}(\rho) = BJ_1(k\rho) \tag{32}$$

$$h_\varphi^{(1)}(\rho) = (4\pi\sigma_1/ck)BJ_0(k\rho) \tag{33}$$

where σ_1 is the core conductivity, c is the velocity of light, J_0 and J_1 are the Bessel functions of the first kind, $k=(1+i)/\delta_1$, and $\delta_1=c/(2\pi\,\sigma_1\omega)^{1/2}$, A and B are the constants, the subscripts φ and z correspond to the circular longitudinal components of the fields.

Since the magnetic fields satisfy the continuous condition at the core-insulation interface, the distribution of the magnetic fields in the region of the insulation layer can be given [57]:

$$e_z^{(2)}(\rho) = A[J_0(kr_1) + kr_1J_1(kr_1)\log(r_1/\rho)] - e_0 \tag{34}$$

$$h_\varphi^{(2)}(\rho) = (4\pi\sigma_1/ck)(r_1/\rho)AJ_1(kr_1) \tag{35}$$

$$e_\varphi^{(2)}(\rho) = B[k(\rho^2 - r_1^2)J_0(kr_1)/2 + r_1J_1(kr_1)]/\rho \tag{36}$$

$$h_\varphi^{(2)}(\rho) = (4\pi\sigma_1/ck)BJ_0(kr_1) \tag{37}$$

where r_1 is the diameter of conductive Cu core. It is worthy to note that Maxwell equations can be reduced to two coupled differential equations for the magnetic field components within the magnetic shell [58-59].

The distribution of the magnetic fields outside the wire can be expressed as [57]:

$$e_z^{(4)}(\rho) = G \log(1/\rho) \tag{38}$$

$$h_\varphi^{(4)}(\rho) = -i(c/\omega)G/\rho \tag{39}$$

Here G is the constant and l is the length of the composite wire.

Furthermore, the diagonal component of the Ni$_{80}$Fe$_{20}$/SiO$_2$/Cu composite wire impedance Z_{zz} can be calculated as the ratio of the applied potential difference le_0 to the total current flowing through the core [60]:

$$Z_{zz} = le_0 / 2\pi\sigma_1 r_1 A J_1(kr_1) \tag{40}$$

The off-diagonal impedance Z_{jz} is defined as the ratio of the pick-up coil voltage to the total current in the Ni$_{80}$Fe$_{20}$/SiO$_2$/Cu composite wire, which is proportional to the off-diagonal component of the surface impedance tensor [58-59]:

$$Z_{\varphi z} = (4\pi N/c) \times [e_\varphi^{(3)}(r_3)]/h_\varphi^{(3)}(r_3)] \tag{41}$$

where N is the number of turns in the pick-up coil, r_3 the radius of the Ni$_{80}$Fe$_{20}$/SiO$_2$/Cu composite wire.

Hence, based on the analysis of the distribution of magnetic fields and the impedance in the Ni$_{80}$Fe$_{20}$/SiO$_2$/Cu composite wire, it can be found that the eddy currents induced and the diagonal Z_{zz} and off-diagonal impedance $Z_{\varphi z}$ in the ferromagnetic shell are enhanced with the addition of the insulation layer, which partially explains why the MI ratio in the Ni$_{80}$Fe$_{20}$/SiO$_2$/Cu composite wire is much higher than that in the Ni$_{80}$Fe$_{20}$/Cu composite wire.

On the other hand, the enhancement in MI ratio of the Ni$_{80}$Fe$_{20}$/SiO$_2$/Cu composite wire can be explained by that the adding of the insulation layer might improve the magnetic properties such as the softness of the ferromagnetic NiFe layer.
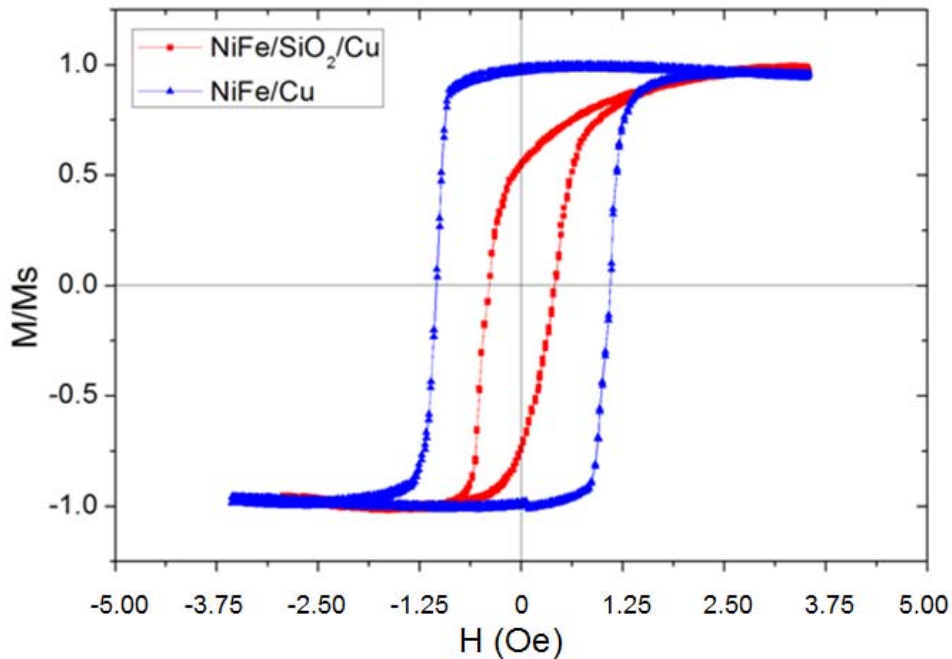
Fig. 22 hysteresis loops of Ni$_{80}$Fe$_{20}$ /SiO$_2$/Cu and Ni$_{80}$Fe$_{20}$/Cu composite wires

Fig. 22 shows the hysteresis loops of Ni$_{80}$Fe$_{20}$/SiO$_2$/Cu and Ni$_{80}$Fe$_{20}$/Cu composite wires. It can be seen that the coercivity of the Ni$_{80}$Fe$_{20}$/SiO$_2$/Cu composite wire and the Ni$_{80}$Fe$_{20}$/Cu composite wire is 0.35 and 1.075, respectively, which indicates that the softness of the NiFe layer was greatly improved in the Ni$_{80}$Fe$_{20}$/SiO$_2$/Cu composite wire.

Moreover, it can be clearly observed in Fig. 22 that the anisotropy of the wires with and without the insulation layer is distinctive. The shape of hysteresis loop of the Ni$_{80}$Fe$_{20}$/SiO$_2$/Cu composite wire is more rounded in comparison with that of the Ni$_{80}$Fe$_{20}$/Cu composite wire. In other words, the anisotropy of

_____

NiFe layer in the $Ni_{80}Fe_{20}$/SiO₂/Cu composite wire tends to be more circumferential instead of being longitudinal in the $Ni_{80}Fe_{20}$/Cu composite wire. This phenomenon can also be proven in Fig. 21. The MI curve of $Ni_{80}Fe_{20}$/SiO₂/Cu composite wire in Fig. 21 displays a double peak, while a single peak is obtained in the MI curve of $Ni_{80}Fe_{20}$/Cu composite wire so that the easy direction of $Ni_{80}Fe_{20}$ ferromagnetic layer in the $Ni_{80}Fe_{20}$/SiO₂/Cu composite wire inclines toward the circumferential direction.

It is well known that the circumferential anisotropy and improved softness of the ferromagnetic NiFe layer could make contribution to the enhancement of GMI effect [59]. Considering all the experimental conditions were the same for both wires, it must be the addition of the insulation layer that is responsible for the reduction in the coercivity and the circumferential anisotropy in the $Ni_{80}Fe_{20}$/SiO₂/Cu composite wire. Therefore, it can be concluded that the addition of the insulation layer exerts great effort on the rise of MI ratio in the $Ni_{80}Fe_{20}$/SiO₂/Cu composite wire by improving the magnetic properties of $Ni_{80}Fe_{20}$ layer.

4.2. Frequency Dependence of GMI Effect in Composite Wires

Fig. 23 presents the frequency dependence of the maximum MI ratios in $Ni_{80}Fe_{20}$/SiO₂/Cu and $Ni_{80}Fe_{20}$/Cu composite wires. It can be seen that the trend of both curves are similar. Furthermore, the maximum MI ratios in both wires appear in the low frequency, which can be explained by that the electromagnetic interaction in both composite structures could enhance the skin effect in the magnetic coatings, even at the low frequencies [61].
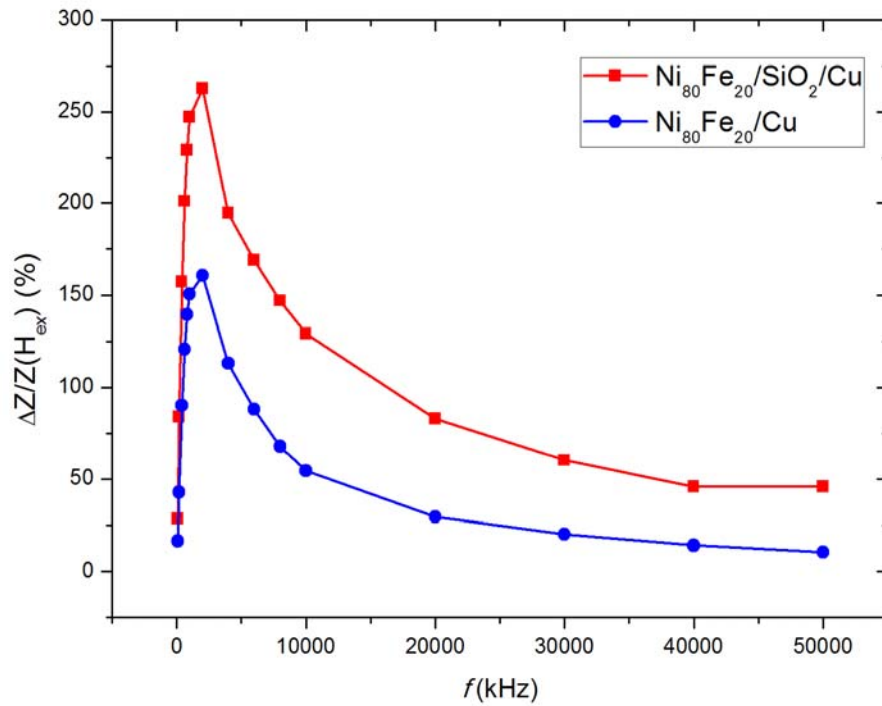
Fig. 23 the frequency dependence of the maximum MI ratios of
Ni$_{80}$Fe$_{20}$/SiO$_2$/Cu and Ni$_{80}$Fe$_{20}$/Cu composite wires

However, it can be observed that the MI ratio of the Ni$_{80}$Fe$_{20}$/SiO$_2$/Cu composite wire increased dramatically over 400 kHz compared to the Ni$_{80}$Fe$_{20}$/Cu composite wire. This phenomenon might be correlated with the change in the circular electric field caused by the addition of the insulation layer in the Ni$_{80}$Fe$_{20}$/SiO$_2$/Cu composite wire. The presence of the insulation layer trends to lead the circular electric field in the NiFe layer to be much higher than the circular electric field in the Cu core so as to encourage the growth of the impedance at higher frequencies.

In addition, the MI curve of the Ni$_{80}$Fe$_{20}$/SiO$_2$/Cu composite wire exhibits the shape of double peak between 2 MHz and 10 MHz, while the Ni$_{80}$Fe$_{20}$/Cu composite wire displays the single peak in the same range (Fig. 24). This

_____

might be explained that the influence of the addition of insulation layer on the magnetic properties of NiFe ferromagnetic layer, such as the anisotropy, inclines to be conspicuous in this frequency range. This conclusion may play significant role in choosing the working frequency in micro magnetic sensors.
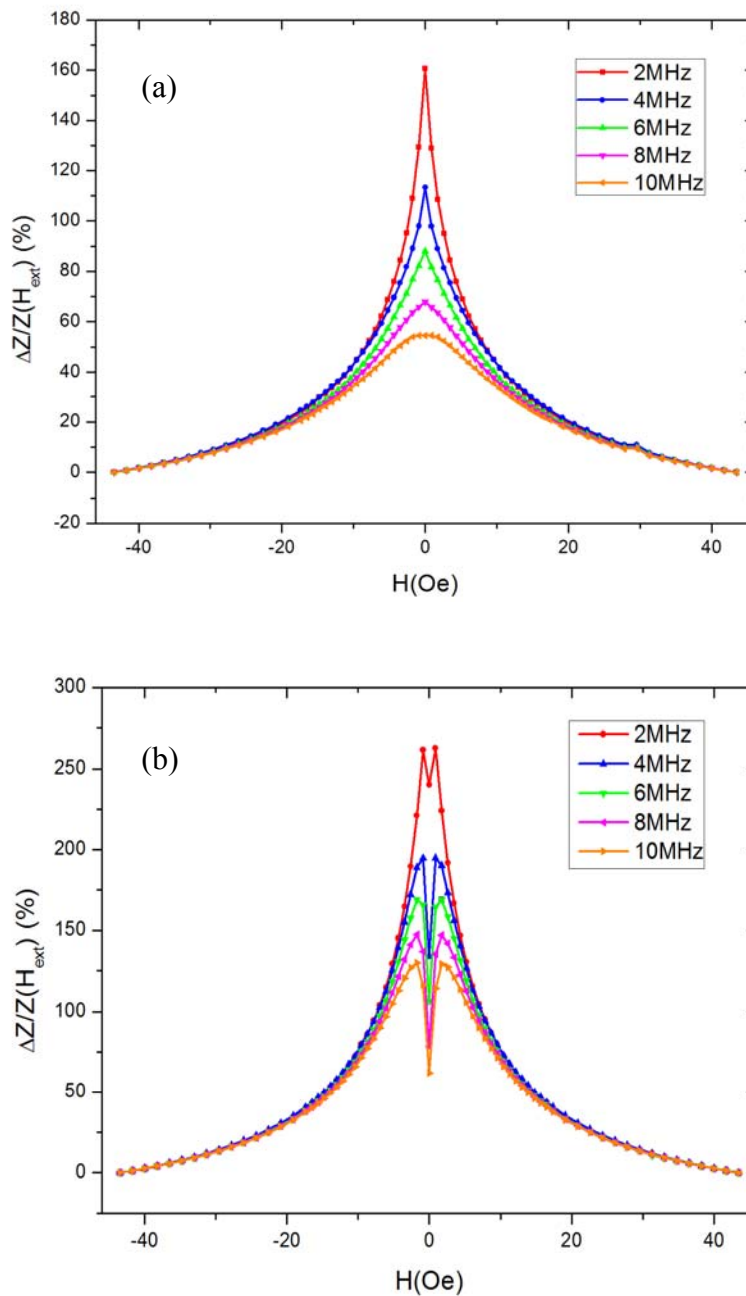
Fig. 24 the frequency dependence of the peak field in Ni$_{80}$Fe$_{20}$/Cu (a) and Ni$_{80}$Fe$_{20}$//SiO$_2$/Cu (b) composite wires between 2 MHz and 10 MHz

_____

4.3. Summary

In this chapter, the GMI effect in the Ni$_{80}$Fe$_{20}$/SiO$_2$/Cu composite wire was studied in comparison with the Ni$_{80}$Fe$_{20}$/SiO$_2$/Cu composite wire in terms of the field dependency and frequency dependency of MI ratio.

The GMI effect in the Ni$_{80}$Fe$_{20}$/SiO$_2$/Cu composite wire caused by the addition of the insulation layer is much higher than that in the Ni$_{80}$Fe$_{20}$/Cu composite wire. The presence of the insulation layer not only increases the eddy current and impedance of the NiFe layer in the Ni$_{80}$Fe$_{20}$/SiO$_2$/Cu composite wire, but also improves the magnetic properties, such as the softness and anisotropy, of the NiFe layer. The distributions of magnetic fields and the enhancement in the diagonal and off diagonal impedance in the Ni$_{80}$Fe$_{20}$/SiO$_2$/Cu composite wire were studied based on Maxwell equations and the magnetic properties of the NiFe layer were analyzed according to hysteresis loops.

Both Ni$_{80}$Fe$_{20}$/SiO$_2$/Cu and Ni$_{80}$Fe$_{20}$/Cu composite wires display the high GMI effect at low frequencies due to the skin effect. In the Ni$_{80}$Fe$_{20}$/SiO$_2$/Cu composite wire, the MI ratio increased dramatically over 400 kHz because the addition of the insulation layer enhanced the circular electric field in the NiFe layer to give rise to the growth of the impedance at higher frequencies. At the same time, a preferential frequency range (2 MHz and 10 MHz) showing superior magnetic properties was found in the Ni$_{80}$Fe$_{20}$/SiO$_2$/Cu composite wire, which might provide high sensing performance in micro magnetic sensors.

Chapter 5

Investigation of Optimum Parameters of Insulation Layer in NiFe/SiO$_2$/Cu Composite Wire

It has been found that the addition of insulation layer between the ferromagnetic layer NiFe and the conductive Cu core is capable of enhancing the GMI effect of Ni$_{80}$Fe$_{20}$/SiO$_2$/Cu composite wire by affecting the diagonal and off-diagonal impedance and the magnetic properties of the NiFe layer. However, the study of the thickness effect of the insulation layer on the magnetic properties of Ni$_{80}$Fe$_{20}$/SiO$_2$/Cu composite wire is virtually non-existed although it has been theoretically speculated that the thickness of insulation layer could influence the distribution of eddy current and the impedance of the ferromagnetic layer NiFe based on Maxwell equations [57]. Hence, the investigation and optimization of the thickness effect of insulation layer in the Ni$_{80}$Fe$_{20}$/SiO$_2$/Cu composite wire were conducted in this chapter.

5.1. Investigation of Thickness Effect of SiO$_2$ Insulation Layer

In order to investigate the existence of the thickness effect of insulation layer on the magnetic properties and sensing performance of Ni$_{80}$Fe$_{20}$/SiO$_2$/Cu composite wire, two Ni$_{80}$Fe$_{20}$/SiO$_2$/Cu composite wires, *Composite Wire A and B*, with larger difference in the thickness of insulation layer were developed. Specifically, the thicknesses of insulation layers in the ranges of micron and nanometer were studied firstly to determine the rough optimized

_____

thickness for the insulation layer.

For Ni$_{80}$Fe$_{20}$/SiO$_2$/Cu composite wire A (*Composite Wire A*), the glass-coated melt spinning process was employed to fabricate the thick insulation layer SiO$_2$ of 10 μm; while a thin insulation layer of 100 nm was developed in the Ni$_{80}$Fe$_{20}$/SiO$_2$/Cu composite wire B (*Composite Wire B*) by the magnetron sputtering method. The role of SiO$_2$ was to insulate the interaction of the magnetic core and the ferromagnetic layer NiFe, therefore the fabrication method of the insulation does not affect results. Besides the distinguish in the thickness of insulation layer, all other experimental details were the same for both wires, namely the diameter of the copper core was 20 μm, the thickness of NiFe layer was 1.5 μm, the electroplating current density was fixed at 2 A/dm^2 and the composition of NiFe layer was 80:20 for both wires. The schematic diagram of the *Composite Wire A* and *B* are shown in Fig. 25.
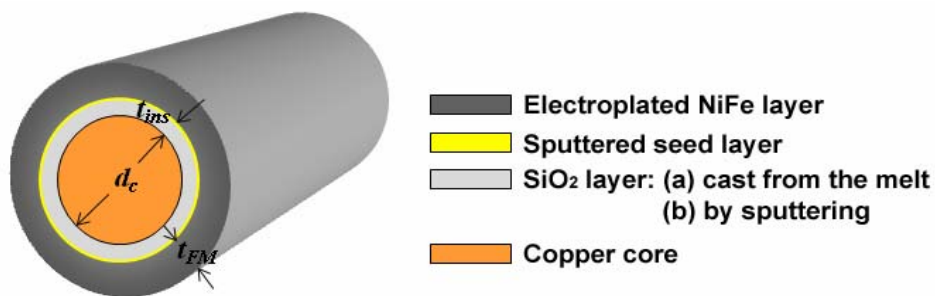
Fig. 25 schematic diagram of *Composite Wire A and B*, where d_c is the diameter of copper core, t_{ins} is the thickness of SiO$_2$ layer, and t_{FM} is the thickness of NiFe layer

The magnetic properties in terms of the magneto-impedance (MI) effect and hysteresis loop for each sample were tested. Due to the MI effect is related to the variation of the magnetic permeability of the plated NiFe layer, and the magnetic permeability is a comprehensive measure of the soft magnetic

properties of the material, the soft magnetic properties of the plated samples can be compared using the maximum MI effect ratios of the wire samples.

Fig. 26 displays the maximum magneto-impedance testing result of *Composite Wire A* and *B*. It can be seen that the maximum MI ratio of *Composite Wire A* is about 132.33 %, which is much larger than that achieved in *Composite Wire B*, 38.45 %. It implies that the thickness of the insulation layer plays an essential role in the overall magnetic properties of Ni$_{80}$Fe$_{20}$/SiO$_2$/Cu composite wire by affecting greatly the interaction between the ferromagnetic shell and the copper core. It also suggests that the thickness of insulation layer above the magnitude of micro should be chosen for the improved sensing performance of Ni$_{80}$Fe$_{20}$/SiO$_2$/Cu composite wire in the applications of magnetic sensing, where magnetic composite wires are used as the critical sensing elements.
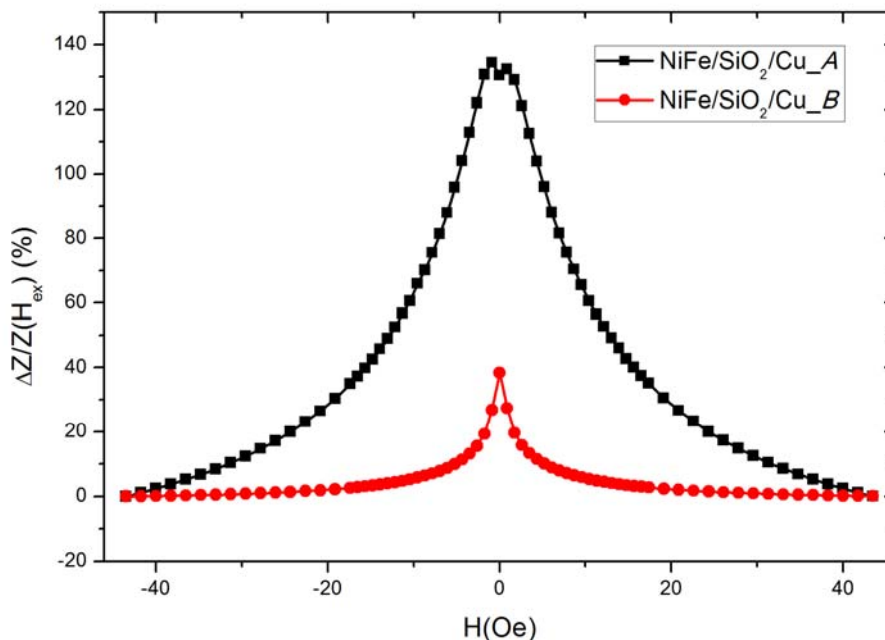
Fig. 26 the maximum MI testing result of *Composite Wire A and B*

_____

Furthermore, for *Composite Wire A*, the MI curve exhibits the double-peak pattern, namely the maximum MI ratio increases initially with H_{ext} to a peak when H_{ext} equals the anisotropy field, H_k, and then falls with further increases of the field, which indicates that the moment rotations dominate the magnetization process in the Ni$_{80}$Fe$_{20}$ layer. Therefore, the circumferential permeability increases with increasing external field until reaching the anisotropy field so that the GMI effect could be enhanced accordingly. After reaching the maximum value of the circumferential permeability, the circumferential permeability decreases with increasing H_{ext}, until the magnetization is saturated. On the contrary, for *Composite Wire B*, a single-peak pattern of the maximum MI curve was obtained, suggesting that the domain wall displacement dominates the magnetization process in the Ni$_{80}$Fe$_{20}$ layer, which results in the monotonic decease of the total circumferential permeability with respect to the external field. In turn, *Composite Wire B* shows a much lower MI ratio. The difference in anisotropy of *Composite Wire A* and *B* can be observed in Fig. 27.
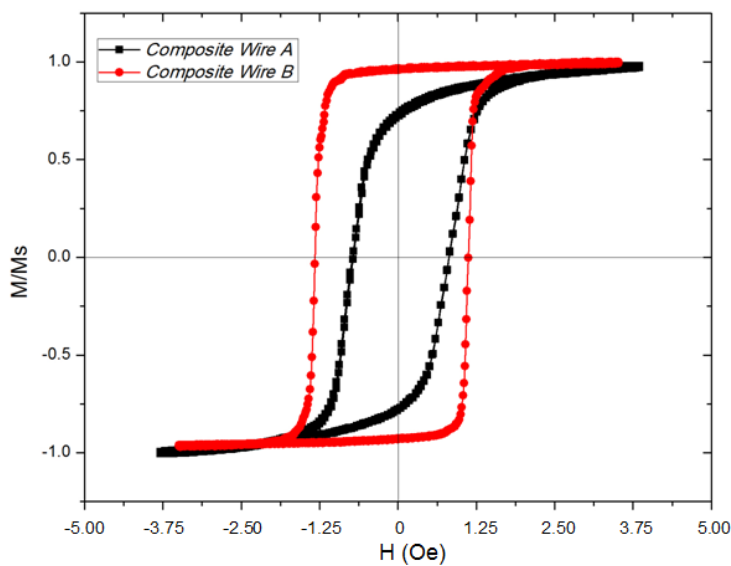
Fig. 27 hysteresis loops of *Composite Wire A and B*

5.2. Optimization of Thickness Effect of Insulation layer SiO$_2$

It has been found that the thickness of the insulation layer has a significant impact on the magnetic properties of Ni$_{80}$Fe$_{20}$/SiO$_2$/Cu composite wire and the promising range of the thickness of insulation layer should fall into the magnitude of micron. Thus, to investigate the optimum thickness of the insulation layer might enable the further enhancement of GMI effect in the Ni$_{80}$Fe$_{20}$/SiO$_2$/Cu composite wire as well as its sensing performance.

In this experiment, a range of Ni$_{80}$Fe$_{20}$/SiO$_2$/Cu composite wires were fabricated with various thicknesses of SiO$_2$ insulation layers, which were 3.2, 5.0, 8.4, and 12.1 µm; the diameter of Cu cores was kept at 20 µm and the Ni$_{80}$Fe$_{20}$ layers were electroplated with the same thickness of 2 µm in all specimens by the manipulation of current density and plating duration.
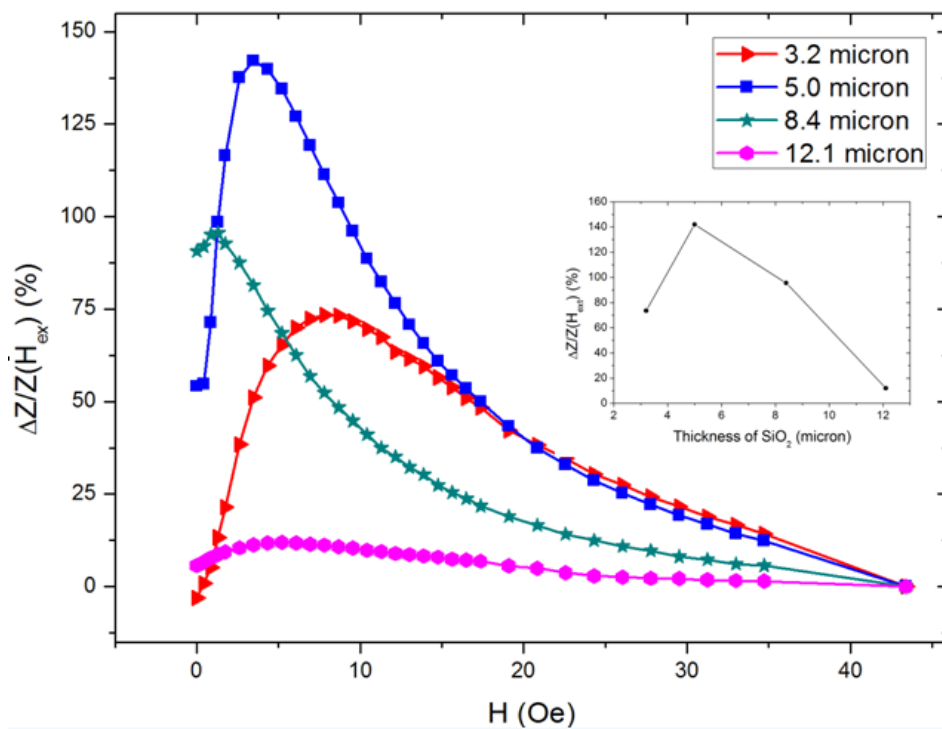
Fig. 28 the maximum MI curves of Ni$_{80}$Fe$_{20}$/SiO$_2$/Cu composite wires with different thicknesses of insulation layers; the inset displays the maximum MI ratio of Ni$_{80}$Fe$_{20}$/SiO$_2$/Cu composite wires.

_____

Fig. 28 shows that the maximum MI curves of Ni$_{80}$Fe$_{20}$/SiO$_2$/Cu composite wires with different thicknesses of insulation layers. It can be observed that the maximum MI ratio of the Ni$_{80}$Fe$_{20}$/SiO$_2$/Cu composite wire enhances firstly with the increase in the thickness of insulator layer. The optimum thickness of the insulation layer, 5.0 μm is obtained, where the highest MI ratio, 142.15%, was achieved. However, further augmentation of the thickness of insulation layer will lead to the decease in MI ratio. The maximum MI ratio of Ni$_{80}$Fe$_{20}$/SiO$_2$/Cu composite wire with the thickness of 8.4 μm reduces to 95.65 % and then markedly plummets to 13.32% at the insulation thickness of 12.1 μm.

This trend can be attributed to the influence of the thickness of insulation layer on the electromagnetic interactions between the Cu core and the magnetic coating. An accessional coupling capacitance was formed between the conductive Cu copper and the ferromagnetic Ni$_{80}$Fe$_{20}$ layer by the addition of the insulation layer SiO$_2$, namely the insulation layer in Ni$_{80}$Fe$_{20}$/SiO$_2$/Cu composite wire acts as a dielectric layer [61], which might be responsible for the enhancement of GMI effect with the increase in the thickness of insulation layer.

On the other hand, when the ac driving current flowed through the Cu core, an ac magnetic field was induced in the magnetic coating and the average magnetic field can be described as:

$$H_\phi = \frac{I_m}{2\pi(R_2 + (t_m/2))} \tag{42}$$

_____

where I_m is the value of the ac driving current, R_2 is the radius of the SiO_2/Cu composite wire, t_m is the thickness of the magnetic layer. It can be found that the magnetic field will decrease on the rise of the thickness of the insulation layers so that the dynamic magnetic permeability in the $Ni_{80}Fe_{20}$ layer decreases to reduce the impedance of the composite wire. In other words, with the increase of the thickness of the insulation layer, a decrease of the eddy current induced in the NiFe shell.

Hence, it can be concluded that the competition between the dielectric layer effect induced by the insulation layer and the influence of the ac magnetic field produces an optimum thickness of SiO_2 insulation layer, 5.0 μm, in this study. When the thickness of the insulation layer is below 5.0 μm, the dielectric layer effect dominates, which enhance the MI ratio with the increase of the thickness of the insulation layer; on the other hand, if the thickness of the insulation layer is beyond 5.0 μm, the impedance of the $Ni_{80}Fe_{20}$/SiO_2/Cu composite wire will drop due to the reduction in dynamic magnetic permeability in the $Ni_{80}Fe_{20}$ layer.

Furthermore, it can be observed in Fig. 28 that the maximum MI ratios of $Ni_{80}Fe_{20}$/SiO_2/Cu composite wire samples reach at different peak field H_k (approximately the anisotropy field). The trend of peak field in $Ni_{80}Fe_{20}$/SiO_2/Cu composite wires is illustrated in Fig. 29.

_____
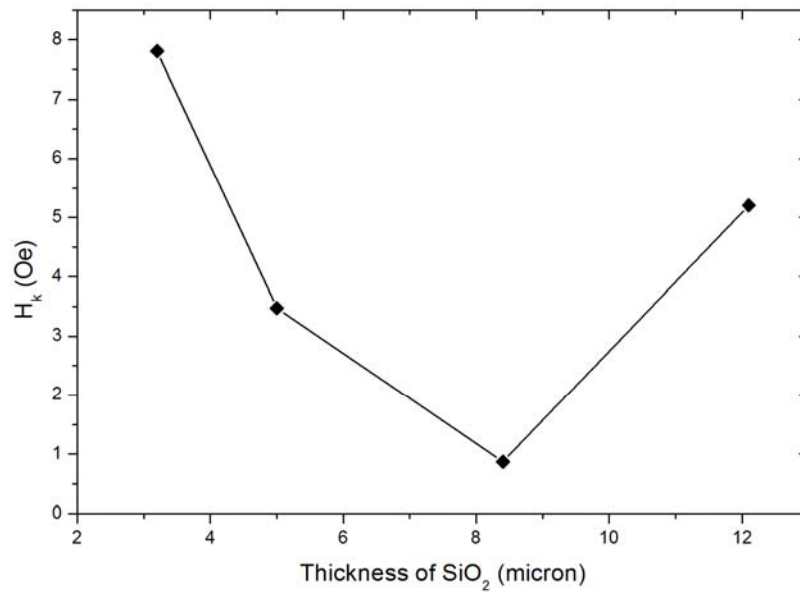
Fig. 29 the peak field H_k for Ni$_{80}$Fe$_{20}$/SiO$_2$/Cu composite wires with different thicknesses of insulation layers

The peak field firstly decreases with the rise of the thickness of the insulation layer, from 7.82 Oe at the thickness of 3.2 μm to 3.45 Oe at 5.0 μm, and then achieves the minimum value of 0.88 Oe at 8.4 μm; beyond the thickness of 8.4 μm, it increases dramatically to 5.19 Oe at 12.1 μm, which demonstrates that the thickness of insulation layer could affect the effective circumferential permeability of the NiFe layer in the Ni$_{80}$Fe$_{20}$/SiO$_2$/Cu composite wire.

Two types of magnetization processes, domain wall movement and magnetic moment rotation, play the essential role in affecting the effective circumferential permeability. The dominance of domain movement will lead the NiFe layer longitudinally, namely showing the low peak field; while the magnetic moment rotation will give rise to the increase of the peak field in the NiFe layer. Hence, it can be found that the increase in the thickness of insulation layer will cause the fall of magnetic moment rotation at certain

_____

range, but further augmentation of the thickness of the insulation layer will cause the enhancement of magnetic moment rotation.

In addition, the thickness of the insulation layer also affects the frequency of the maximum MI ratio in Ni$_{80}$Fe$_{20}$/SiO$_2$/Cu composite wires. Fig. 30 illustrates the relationship between the frequency and the maximum MI ratio of Ni$_{80}$Fe$_{20}$/SiO$_2$/Cu composite wires with various thicknesses of insulation layers. It can be seen that the frequency of the maximum MI ratio of Ni$_{80}$Fe$_{20}$/SiO$_2$/Cu composite wire decreases with the rise of thickness of the insulation layers. The maximum MI ratio in Ni$_{80}$Fe$_{20}$/SiO$_2$/Cu composite wire with the thickness of 3.2 μm is obtained at 2 MHz, and then the frequency of the maximum ratio gradually drops to 600 kHz as the thickness of the insulation layer increases to 12.1 μm.
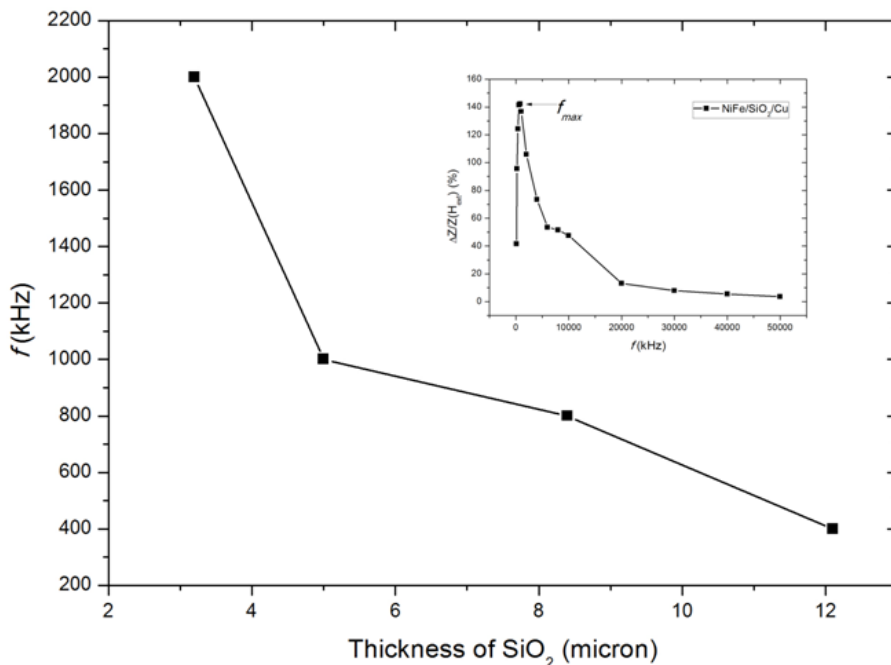
Fig. 30 the relationship between the frequency and the maximum MI ratio of Ni$_{80}$Fe$_{20}$/SiO$_2$/Cu composite wires with various thicknesses of the insulation layers; the inset shows the frequency dependence of MI ratio in the Ni$_{80}$Fe$_{20}$/SiO$_2$/Cu composite wire with the thickness of 5 μm.

_____

It is well known that GMI effect originates from the skin effect and it had been proven that the electromagnetic interactions between the ferromagnetic NiFe shell and the conductive core is capable of improving the skin effect in NiFe/Cu composite wires [63], which enables the GMI effect to be seen at relatively low frequency. The function of the skin depth for homogeneous materials is as:

$$\sigma_m = f(\frac{2}{\omega\mu_\phi\sigma})$$ (43)

where μ_Φ is the dynamic circumferential permeability in the magnetic layer, σ is the conductivity and ω is the angular frequency of ac current. The initial frequency f_0 is determined when the skin depth is equal to the radius of the composite wire.

According to Fig. 30, it can be seen that the addition of the insulation could further enhance the skin effect as the increase in the thickness of the insulation layer. The characteristic frequency f_{max} can be roughly calculated from the condition as:

$$f_{max} = f(\frac{1}{\mu_{\phi S}\pi d^2\sigma})$$ (44)

where d is the diameter and $\mu_{\Phi S}$ is the saturated permeability in the magnetic field.

_____

5.3. Summary

A range of $Ni_{80}Fe_{20}/SiO_2/Cu$ composite wires with various thicknesses of SiO_2 insulation layers were developed and the thickness effect of the insulation layer SiO_2 on the GMI effect was investigated in this chapter.

In order to investigate the existence of the thickness effect of insulation layer on the magnetic properties and sensing performance of the $Ni_{80}Fe_{20}/SiO_2/Cu$ composite wire, the two $Ni_{80}Fe_{20}/SiO_2/Cu$ composite wires, $Ni_{80}Fe_{20}/SiO_2/Cu$ *Composite Wire A* and *B*, with larger difference in the thickness of insulation layer (10 μm for *Composite Wire A* and 100 nm for *Composite Wire B*) were developed. It was discovered that the maximum MI ratio of *Composite Wire A* (132.33 %) is much larger than that of *Composite Wire B* (38.45 %) due to the enhancement of the interaction between the ferromagnetic shell and the copper core by the thick insulation layer. Moreover, the double-peak pattern of maximum MI curve in *Composite Wire A* in comparison with the single-peak pattern for *Composite Wire B* was found, which indicates that the increase in the thickness of insulation layer could improve the circumferential permeability of the $Ni_{80}Fe_{20}/SiO_2/Cu$ composite wire so as to enhance its GMI effect and sensing performance.

Furthermore, the optimization of the thickness effect of the insulation layer SiO_2 in the $Ni_{80}Fe_{20}/SiO_2/Cu$ composite wire was conducted. In the experiment, four $Ni_{80}Fe_{20}/SiO_2/Cu$ composite wires with the thickness of SiO_2 of 3.2, 5.0, 8.4, and 12.1 μm were fabricated under the same experimental conditions. It was observed that the maximum MI ratio of the

_____

$Ni_{80}Fe_{20}/SiO_2/Cu$ composite wire enhanced firstly with the increase in the thickness of insulator layer from 3.2 to 5.0 μm, and then dropped from 5.0 to 12.1 μm due to the competition between the dielectric layer effect induced by the insulation layer and influence of ac magnetic field. An optimum thickness of insulation layer SiO_2, 5.0, was obtained, where the highest MI ratio 142.15% was achieved in this study.

Moreover, the relationship between the thickness of SiO_2 and the peak field of the maximum MI ratio was studied. The conclusion was drawn that the increase in the thickness of the insulation layer will cause the fall of magnetic moment rotation at certain range, but further augmentation of the thickness of the insulation layer will give rise to the enhancement of magnetic moment rotation.

In addition, the trend of the thickness of SiO_2 and the frequency of the maximum MI ratio in $Ni_{80}Fe_{20}/SiO_2/Cu$ composite wires was investigated. It was concluded that the addition of the insulation could further enhance the skin effect as the increase in the thickness of insulation layer so as to decrease the frequency of the maximum MI ratio in $Ni_{80}Fe_{20}/SiO_2/Cu$ composite wires.

Chapter 6

Enhancement of Magnetic Properties and Sensing Performance of NiFe/SiO$_2$/Cu Composite Wires in relation to the NiFe Layer

In order to achieve the optimum performance of the Ni$_{80}$Fe$_{20}$/SiO$_2$/Cu composite wire, the improved parameters for the insulation layer SiO$_2$ have been obtained in chapter 5. However, the study of the effect of Ni$_{80}$Fe$_{20}$ ferromagnetic layer on the magnetic properties and sensing performance of the Ni$_{80}$Fe$_{20}$/SiO$_2$/Cu composite wire has not been discussed. Thus, the investigation and characterization of the Ni$_{80}$Fe$_{20}$ ferromagnetic layer will be conducted in this chapter to optimize the Ni$_{80}$Fe$_{20}$/SiO$_2$/Cu composite wire further.

6.1. Study of Thickness Proportion of NiFe and SiO$_2$ Layers

In this study, the investigation of the optimum proportion of the thicknesses of the SiO$_2$ insulation layer and the Ni$_{80}$Fe$_{20}$ ferromagnetic layer was carried out. A series of Ni$_{80}$Fe$_{20}$/SiO$_2$/Cu composite wire samples were synthesized with the same Cu cores of 20 μm in diameter and the equal thickness of SiO$_2$ insulation layers of 5 μm. The plating current density J was fixed at 2 A/dm^2 and the composition ratio of Ni$_{80}$Fe$_{20}$ was controlled by adjusting Ni^{2+}/Fe^{2+} ion ratio of the electrolyte solution and was verified using EDX. The thicknesses of Ni$_{80}$Fe$_{20}$ ferromagnetic layers, 1.5, 2.9, 4.5, 6.0, and 7.5 μm, were obtained

_____

by manipulating the plating duration, thus a range of thickness proportions of NiFe and SiO$_2$ layers (Φ), 0.3, 0.58, 0.9, 1.2 and 1.5, were calculated accordingly.
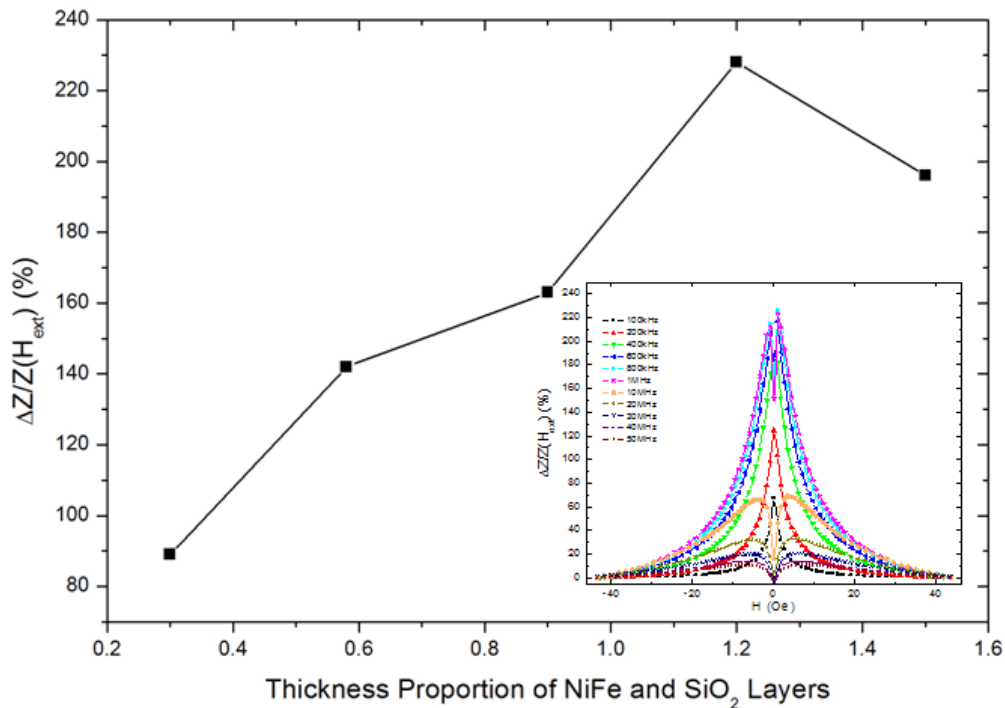
Fig. 31 the maximum MI ratios of Ni$_{80}$Fe$_{20}$/SiO$_2$/Cu composite wire samples with various thickness proportions of NiFe and SiO$_2$ layers; the inset shows that field dependence of MI curve of the Ni$_{80}$Fe$_{20}$/SiO$_2$/Cu composite wire with the thickness of NiFe and SiO$_2$, 5.0 and 6.0 μm, respectively.

It can be seen in Fig. 31 that the maximum MI ratio initially increases with the increase in the thickness proportion of NiFe and SiO$_2$ layers, from 89% to 228 %, and then falls to 196% where the thickness proportion of NiFe and SiO$_2$ layers is 1.5. An optimum Φ, 1.2, was obtained, namely the thickness of NiFe and SiO$_2$ layers is 6.0 and 5.0 μm, respectively.

The trend of the maximum MI ratio may partially due to the increase in the coating thickness of NiFe layer. Fig. 32 presents the coercivity over the thickness of all samples. It can be seen that the coercivity H_c decreases from

0.63 to 0.365 with the rise of the thickness of the NiFe layer, which indicates

that the soft magnetic properties of the ferromagnetic layer NiFe have been

improved so that the initial improvement of the GMI effect is realized since

coercivity and permeability has an inverse relationship with each other [64].

Moreover, it can be observed in Fig. 32 inset that the increase in the thickness

of NiFe layer leads to a preferential circumferential magnetic structure, where

the magnetic moment rotation dominated the magnetization process, which

can also contribute the enhancement of GMI effect of Ni$_{80}$Fe$_{20}$/SiO$_2$/Cu
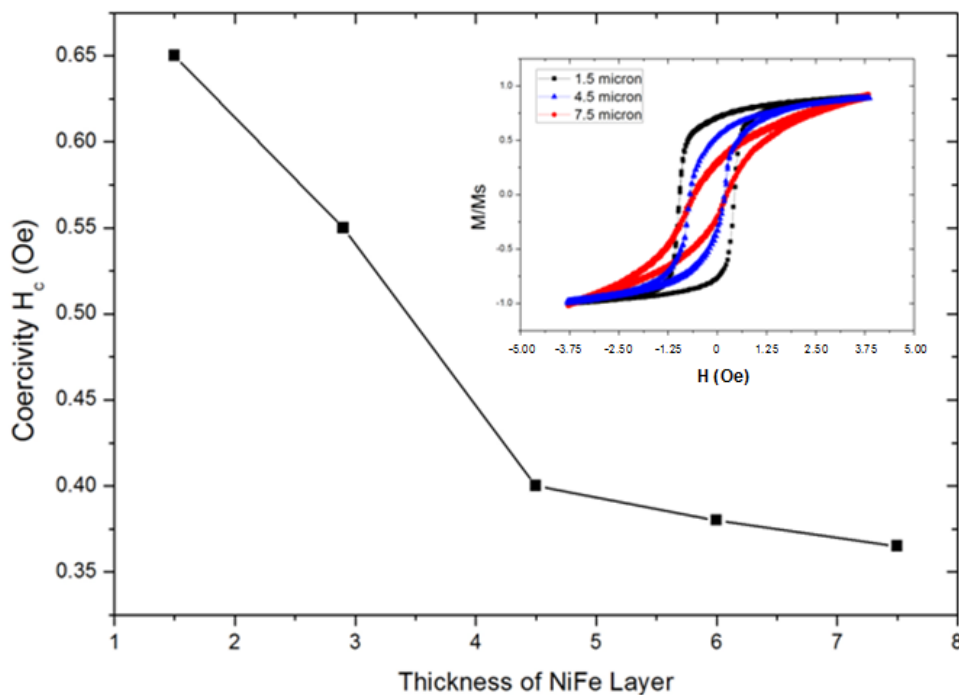
composite wire.

Fig. 32 the coercivity of Ni$_{80}$Fe$_{20}$/SiO$_2$/Cu composite wires with different
thicknesses of NiFe layers; the inset displays the hysteresis loops of
Ni$_{80}$Fe$_{20}$/SiO$_2$/Cu composite wires.

Furthermore, the relationship between impedance, Z, of the material and the

skin depth δ can be given:

$$Z : \frac{1}{\delta} \tag{45}$$

In the Ni$_{80}$Fe$_{20}$/SiO$_2$/Cu composite wire, the skin depth can be sharply affected by the addition of insulation layer since the insulation layer plays an essential role in the distribution of eddy current as stated in chapter 4. It is also well established that if the skin depth δ is thicker than or near the thickness of NiFe layer, a lower MI ratio will be led to. As a result, the improvement of magnetic properties of NiFe layer as the increase in the thickness and the influence of skin effect in relation to the thickness of NiFe and SiO$_2$ layers form the overall trend of the maximum MI ratios of Ni$_{80}$Fe$_{20}$/SiO$_2$/Cu composite wire samples in Fig. 32 and create the optimum thickness proportion of NiFe and SiO$_2$ layers, 1.2, in this study.

In addition, as the coating thickness was increased from 1.5 μm to 7.5 μm, the frequency, at which the maximum MI occurs, drastically reduced from 4 MHz to 600 kHz. This can be explained by the changes in the skin depth. The effective critical frequency of skin effect is qualitatively described as

$$\omega = \frac{2}{\mu_0 \mu_{eff} \sigma_{eff} r_0^{\,2}} \tag{46}$$

where r_0 is the radius of the composite wire.

6.2. Study of Current Density for Electroplating NiFe Layers

Besides the thickness of the NiFe ferromagnetic layer, the electroplating current density also has a significant impact on the magnetic properties and sensing performance of Ni$_{80}$Fe$_{20}$/SiO$_2$/Cu composite wire since the permeability of the NiFe layer can be markedly affected by its grain size

induced by various plating current density. Therefore, the investigation of the
current density effect in the development of Ni$_{80}$Fe$_{20}$/SiO$_2$/Cu composite wires
by electrodeposition was carried out to improve the magnetic properties and
sensing performance of the composite wire.

In this study, a range of Ni$_{80}$Fe$_{20}$/SiO$_2$/Cu composite wires were developed
under various plating current densities. The current densities adopted in this
experiment are 1, 2, 4, 7, and 11 A/dm^2. The chemical composition and
thickness of NiFe layer were fixed at 80:20 and 1.5 μm by manipulating the
electrolyte solution concentration and the plating duration, which were
verified by SEM and EDX, respectively. The magnetic properties in terms of
the magneto-impedance (MI) effect and hysteresis loop for each of these
samples were tested.
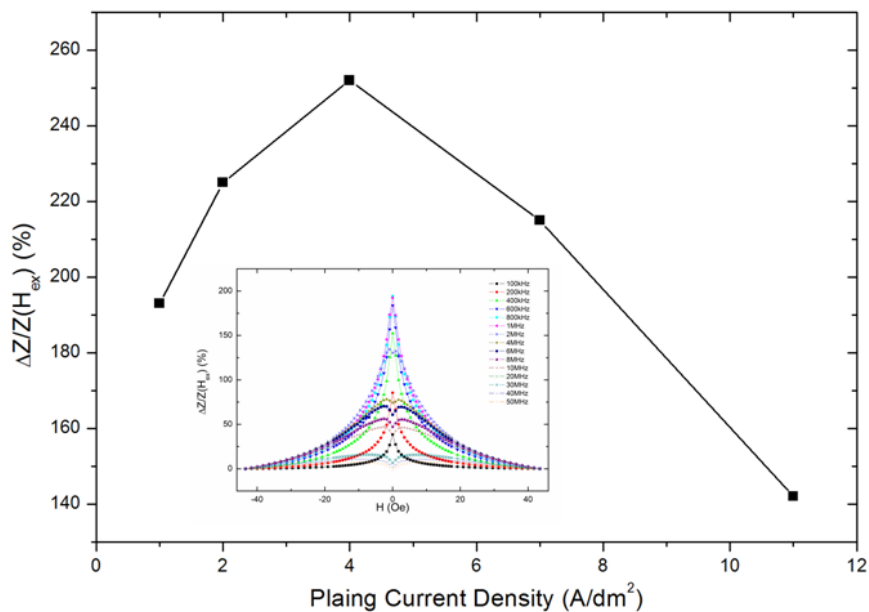
Fig. 33 the maximum MI ratios of Ni$_{80}$Fe$_{20}$/SiO$_2$/Cu composite wires under
various plating current density from 1 to 11 A/dm^2; the inset shows the field
dependence of MI ratio for the composite wire electroplated at 1 A/dm^2 to
illustrate a typical MI curve obtained in this experiment.

_____

Fig. 33 displays the maximum MI ratios of the Ni$_{80}$Fe$_{20}$/SiO$_2$/Cu composite wires plated under a range of current density (from J = 1 A/dm^2 to J = 11 A/dm^2). It can be seen that the maximum MI ratio initially increases with the rise of the plating current density till the J = 4 A/dm^2 and then falls with further augmentation of plating current density.

The increase in MI ratio from 193.35% to 252.33% when the current density rises from 1 to 4 A/dm^2 can be explained by the improved circumferential permeability with the enhancement of plating current density. During the electroplating, a higher current density could generate a stronger circumferential magnetic field around the wire based on the following formula:

$$B_c = \frac{\mu_0 I}{2\pi r} \tag{47}$$

where μ_0 is the permeability in vacuum, r is the distance from the center of the core. Hence, B_c increases linearly with the plating current density. The stronger circumferential magnetic field B_c is capable of leading the magnetic domains in the deposited NiFe layer to a closer alignment to the circumferential direction, which can be evidently proven in Fig. 34, where the maximum MI curves of the Ni$_{80}$Fe$_{20}$/SiO$_2$/Cu composite wires electroplated at 1 and 11 A/dm^2 are presented. It can be clearly seen the composite wire at the plating current density of 11 A/dm^2 exhibits a double peak pattern in comparison with the composite wire at the plating current density of 1 A/dm^2, namely the peak field H_k is larger and more circumferential.
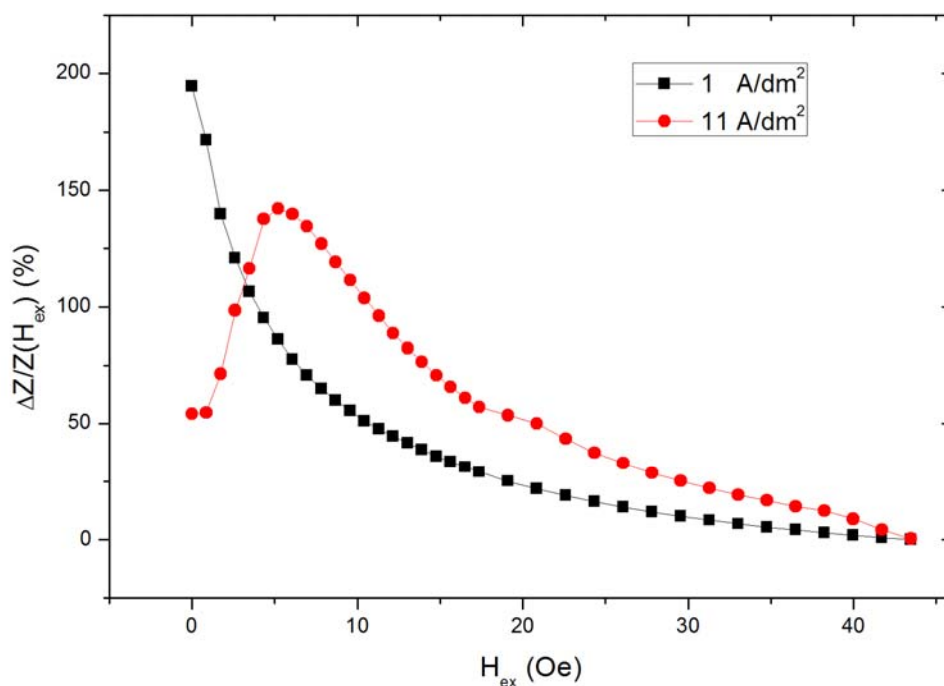
Fig. 34 the maximum MI curves of the $Ni_{80}Fe_{20}/SiO_2/Cu$ composite wires electroplated at 1 and 11 A/dm^2

Although the stronger circumferential magnetic field B_c is able to improve enhance the response of the NiFe layer to the external magnetic field and thus higher MI ratio can be achieved, the increased plating current density might induce larger stresses in the plated NiFe layer, which will reduce the permeability of the plated NiFe [65]. The overall trend of coercivity with increasing the current density can be seen in Fig. 35.

Hence, it can be concluded that the enhancement of circumferential permeability of the NiFe layer induced by the larger current density dominates the GMI effect of the $Ni_{80}Fe_{20}/SiO_2/Cu$ composite wire and leads to the rise of MI ratios before a critical value 4 A/ dm^2; as the plating current density is beyond 4 A/ dm^2, the stress induction by larger current density plays the major

role in the GMI effect of Ni$_{80}$Fe$_{20}$/SiO$_2$/Cu composite wire, which reduces the

MI ratio of the composite wire.
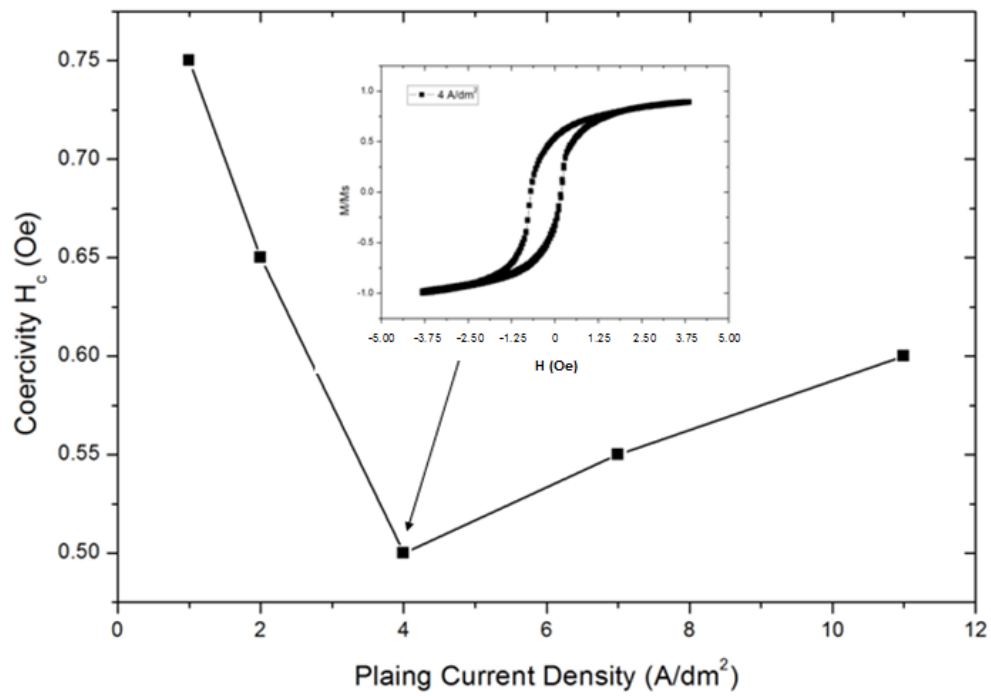
Fig. 35 the coercivity of Ni$_{80}$Fe$_{20}$/SiO$_2$/Cu composite wires with increasing the current density; the inset presents the hysteresis loop of the composite wire with the lowest coercivity.

6.3. Summary

The investigations of the optimum thickness proportion of NiFe and SiO$_2$ layers and the improved current density for electroplating NiFe layer were conducted to achieve the superior magnetic properties and sensing performance of the Ni$_{80}$Fe$_{20}$/SiO$_2$/Cu composite wire in this chapter.

In the study of the optimum thickness proportion of the SiO$_2$ insulation layer and the Ni$_{80}$Fe$_{20}$ ferromagnetic layer, Ni$_{80}$Fe$_{20}$/SiO$_2$/Cu composite wires with the thicknesses of Ni$_{80}$Fe$_{20}$ ferromagnetic layers, 1.5, 2.9, 4.5, 6.0, and 7.5 μm, were fabricated under the same experimental conditions. The thickness of the insulation layer was 5 μm in all samples. It was found that the maximum MI ratio initially increased with the rise of the thickness proportion of NiFe and SiO$_2$ layers, from 89% to 228 %, and then fell to 196% where the thickness proportion of NiFe and SiO$_2$ layers was 1.2, which can be explained by the magnetic properties of NiFe layer was improved with the increase of the coating thickness as so to lead to the lager GMI effect in the beginning and then the influence of skin effect in relation to the thickness of NiFe and SiO$_2$ gave rise to the decrease in MI ratios.

In the experiment of optimizing the electroplating current density, a range of Ni$_{80}$Fe$_{20}$/SiO$_2$/Cu composite wires were developed under various plating current densities, 1, 2, 4, 7, and 11 A/dm^2 with the same chemical composition and thickness of NiFe layer. The optimum plating current density 4 A/dm^2 was observed where the composite displayed the maximum MI ratio. Before reaching the plating current density, the maximum MI ratio initially increased

with the rise of the plating current density which might be due to the enhancement of circumferential permeability of NiFe layer induced by the larger current density; when beyond this critical value, 4 A/dm^2, the maximum MI ratio of composite wires decreased with further augmentation of plating current density since the stress induction by larger current density dominated to lower the permeability of NiFe layer in the Ni$_{80}$Fe$_{20}$/SiO$_2$/Cu composite wire.

Chapter 7

Conclusions and Recommendations

7.1. Conclusions

This thesis mainly focused on the research of super permeability NiFe/SiO$_2$/Cu composite wires for micro magnetic sensor applications. The following conclusions can be drawn:

1. The GMI effect in the NiFe/SiO$_2$/Cu composite wire in relation to the addition of insulation layer SiO$_2$ was studied in terms of the field and frequency dependence of MI curves.

(1) It was discovered that the adding of the insulation layer in the composite wire NiFe/Cu led to the rise of the GMI effect, which can be explained by the increase in the eddy current and the impedance of the NiFe layer in the Ni$_{80}$Fe$_{20}$/SiO$_2$/Cu composite wire induced by the insulation layer as well as the improvement in its magnetic properties, such as the softness and anisotropy by the addition of the insulation layer.

(2) In the study of the frequency dependence of MI curves of NiFe/SiO$_2$/Cu and NiFe/Cu composite wires, it was found that both wires displayed the high GMI effect at low frequencies due to the skin effect. However there was a sharp increase in MI ratio of NiFe/SiO$_2$/Cu composite wire over 400 kHz due to the enhancement in the circular electric field in the NiFe layer by the insulation layer. In addition, the frequency range (2 MHz and 10 MHz) was

69

_____

obtained in the $Ni_{80}Fe_{20}/SiO_2/Cu$ composite wire, showing superior magnetic properties for micro magnetic sensor applications.

2. The investigation of optimum parameters for the insulation layer in the $NiFe/SiO_2/Cu$ composite wires was conducted.

(1) Two $Ni_{80}Fe_{20}/SiO_2/Cu$ composite wires, *Composite Wire A and B*, with the large difference in the thickness of insulation layer (10 μm for *Composite Wire A* and 100 nm for *Composite Wire B*) were developed to investigate the thickness effect of the insulation layer SiO_2 on the GMI effect of the $Ni_{80}Fe_{20}/SiO_2/Cu$ composite wire. The maximum MI ratio of *Composite Wire A* (132.33 %) was obtained in comparison with *Composite Wire B* (38.45 %) due to the enhancement of the interaction between the ferromagnetic shell and the copper core by the thick insulation layer and the increase in the thickness of insulation layer could improve the circumferential permeability of the $Ni_{80}Fe_{20}/SiO_2/Cu$ composite wire.

(2) Four $Ni_{80}Fe_{20}/SiO_2/Cu$ composite wires with the thickness of SiO_2 of 3.2, 5.0, 8.4, and 12.1 μm were fabricated to optimize the thickness effect of insulation layer SiO_2. The optimum thickness of the insulation layer SiO_2, 5.0 μm, was obtained, where the highest MI ratio 142.15% was achieved in this study. Moreover, it was discovered that the increase in the thickness of the insulation layer will cause the drop of the magnetic moment rotation at certain range. In addition, the trend of the thickness of the SiO_2 layer and the frequency of the maximum MI ratio showed that the thicker insulation layer could decrease the frequency of the maximum MI ratio in the $Ni_{80}Fe_{20}/SiO_2/Cu$ composite wire by enhancing the skin effect.

3. The investigation of the optimum thickness proportion of NiFe and SiO_2 layers and the improved current density for electroplating NiFe layer were carried out.

(1) $Ni_{80}Fe_{20}/SiO_2/Cu$ composite wires with the thicknesses of $Ni_{80}Fe_{20}$ ferromagnetic layers, 1.5, 2.9, 4.5, 6.0, and 7.5 μm, and the thickness of 5 μm of insulation layer were fabricated. The optimum thickness proportion of the insulation layer SiO_2 and the ferromagnetic layer $Ni_{80}Fe_{20}$, 1.2, was found, where the maximum MI ratio, 228 %, was obtained. This result can be attributed to the competition between the improvement in the magnetic properties of NiFe layer and the influence of skin effect as the increase in the thickness of the NiFe layer.

(2) The optimized plating current density, 4 A/dm^2, was also achieved in the study of a range of $Ni_{80}Fe_{20}/SiO_2/Cu$ composite wires developed under various plating current densities, 1, 2, 4, 7, and 11 A/dm^2. The creation of the optimum current density was as a result of the domination of two factors induced by the plating current density, namely the enhancement of circumferential permeability by the stronger circumferential magnetic field induced and the reduction in the permeability caused by stress induction in the NiFe layer.

7.2. Recommendations

In this study, the author does not have access to different materials for the study of the insulation layer effect in the composite wire, all insulation layers were fabricated with SiO_2. Since different insulation materials, such as ceramic and alumina, have various dielectric coefficiencies which might lead

_____

to the change in the insulation layer effect in the NiFe/Insulation/Cu composite wire, it is recommended that the investigation of the effect of various types of insulation materials on the magnetic properties and sensing performance of the NiFe/Insulation/Cu composite wire be carried out.

References

[1] Z.J. Zhao, X.P. Li, C. Chua, H.L. Seet, L. Lu, "Effect of annealing on magnetic properties of NiFe/Cu composite wires", *Transactions of the Materials Research Society of Japan* 29(4) 1705-1708 (2004)

[2] Hauser H, Steindl R, Hausleitner C, Pohl A, Nicolics J, "Wirelessly interrogable magnetic field sensor utilizing giant magnetoimpedance effect and surface acoustic wave devices" *IEEE Instrum Meas* 2000;49:648–52.

[3] Manh-Huong Phan, Hua-Xin Peng, "Giant magnetoimpedance materials: Fundamentals and applications", *Progress in Materials Science* 53 (2008) 323–420.

[4] Ripka P: Magnetic sensors and magnetometers, Artech House Publishers, 2001.

[5] Chiriac H, Tibu M, Moga AE, Herea DD, "Magnetic GMI sensor for detection of biomolecules" *J Magn Magn Mater* 2005;293:671–3.

[6] C. Bouligand, J. Dyment, Y. Gallet and G. Hulot, "Geomagnetic field variations between chrons 33r and 19r (83–41 Ma) from sea-surface magnetic anomaly profiles", *Earth and Planetary Science Letters* 250 541–560 (2006)

[7] Gunther Kletetschk, Norman F. Ness, J.E.P. Connerney, M.H. Acuna, P.J. Wasilewski, "Grain size dependent potential for self generation of magnetic anomalies on Mars via thermoremanent magnetic acquisition and magnetic interaction of hematite and magnetite", *Physics of the Earth and Planetary Interiors* 148 149–156 (2005)

References

---

[8] Mohri K, Uchiyama T, Panina PV, "Recent advances of micro magnetic sensors and sensing application", *Sens Acta* A 1997; 59:1–8.

[9] Nesteruk K, Kuzminski M, Lachowicz HK. Novel magnetic field meter based on giant magnetoimpedance (GMI) effect. Sen Trans Mag 2006; 65:515–20.

[10] Florian Kaluza, Angelika Grüger, Heinrich Grüger, "New and future applications of fluxgate sensors", *Sensors and Actuators A* 106 48–51 (2003)

[11] L. Perez, C. Aroca , P. Sánchez , E. López , M.C. Sánchez, "Planar fluxgate sensor with an electrodeposited amorphous core" *Sensors and Actuators A* 109 208–211 (2004)

[12] Hauser H, Steindl R, Hausleitner C, Pohl A, Nicolics J, "Wirelessly interrogable magnetic field sensor utilizing giant magnetoimpedance effect and surface acoustic wave devices" *IEEE Instrum Meas* 2000;49:648–52.

[13] Pohl A, "A review of wireless SAW sensors" *IEEE Trans Ultrason Ferroelectr Frequency Control* 2000; 47:317–32.

[14] Malatek M, Ripka P, Kraus L, "Double-core GMI current sensor", *IEEE Trans Magn* 2005;41:3703–5.

[15] Gonzalez J, Chen AP, Blanco JM, Zhukov A, "Effect of applied mechanical stressses on the impedance response in amorphous microwires with vanishing Magnetostriction", *Phys Stat Sol* A 2002;189:599–608.

[16] Cobeno AF, Zhukov A, Blanco JM, Larin V, Gonzalez J, "Magnetoelastic sensor based on GMI of amorphous microwire" *Sens Acta* A 2001;91:95–8.

[17] Ahn SJ, Kim CG, Park CG, Yu SC, "Laser annealing effect of giant magneto-impedance in amorphous $Co_{66}Fe_4Nib_{14}Si_{15}$ ribbon", *Mater Sci Eng* A 2001;304–306:1026–9.

References

_____

[18] M. Vazquez, "Soft magnetic wires", *Physica B* 299 302-313 (2001)

[19] Ryusuke Hasegawa, "Magnetic wire fabrication and applications", *Journal of Magnetism and Magnetic Materials* 249 346-350 (2002)

[20] Ryusuke Hasegawa, "Design and fabrication of new soft magnetic materials", *Journal of Non-Crystalline Solids* 329 1-7 (2003)

[21] Hans Warlimont, "Amorphous metals driving materials and process innovations", *Materials Science and Engineering A* 304-306 61-67 (2001)

[22] A. Fert, L. Piraux, "Magnetic nanowires", *Journal of Magnetism and Magnetic Materials* 200 338-358 (1999)

[23] F. Borza, T.A. Ovari, T. Meydan, "Mechanical torque in the ac field induced rotation of amorphous wires", *Sensors and Actuators A* 129 224-226 (2006)

[24] H. Chiriac, A.M. Fecioru, T.-A. Ovari, "FMR investigation of surface anisotropy in twisted amorphous wires", *Sensors and Actuators A* 106 251-254 (2003)

[25] N.A. Buznikov, A.S. Antonov, CheolGi Kim, Chong-Oh Kim, A.A. Rakhmanov, Seok-Soo Yoon, "The effect of domain-walls motion on second harmonic amplitude of magnetoinductive response in Co-based amorphous wires", *Journal of Magnetism and Magnetic Materials* 285 101-111 (2005)

[26]L.V. Panina, H. Katoh, K. Mohri, "Magnetization processes in amorphous wires in orthogonal fields", *IEEE Transactions on Magnetics* 29(6) 2524-2526 (1993)

[27] L.V. Panina, K. Mohri, D.P. Makhnovskiy, "Mechanism of asymmetrical magnetoimpedance in amorphous wires", *Journal of Applied Physics* 85(8) 5444-5446 (1999)

References
_____

[28] D. Garcia, V. Raposo, O. Montero, J.I. Iniguez, "Theoretical estimation of magnetoimpedance frequency dependence in amorphous wires", *Journal of Magnetism and Magnetic Materials* 316 e846-e849 (2007)

[29] V. Raposo, D. Garcia, M. Zazo, A.G. Flores, J.I. Iniguez, "Frequency dependence of the giant magnetoimpedance in current annealed amorphous wires", *Journal of Magnetism and Magnetic Materials* 272-276 1463-1465 (2004)

[30] T. Sanchez, P. Alvarez, J. Olivera, M.J. Perez, F.J. Belzunce, J.D. Santos, J.L. Sanchez LI., M.L. Sanchez, P. Gorria, B. Hernando, "Torsion annealing influence on the impedance behaviour in amorphous FeSiB and CoSiB wires", *Journal of Non-Crystalline Solids* 353 914-918 (2007)

[31] T. Meydan, F. Borza, N. Derebasi, "Large gyromagnetic effect in as-cast and post-poduction treated amorphous wires", *Sensors and Actuators A* 106 278-281 (2003)

[32] N. Bayri, S. Atalay, "Giant stress-impedance effect in $Fe_{71}Cr_7Si_9B_{13}$ amorphous wires", *Journal of Alloys and Compounds* 381 245-249 (2004)

[33] H. Chiriac, E. Hristoforou, Maria Neagu, Firuta Barariu, I. Darie, "Inverse wiedemann effect in glass-covered amorphous wires", *Sensors and Actuator*s 81 147-149 (2000)

[34] H. Chiriac, T.A. Ovari, Gh. Pop, Firuta Barariu, "Amorphous glass-covered magnetic wires for sensing applications", Sensors and Actuators A 59 243-252 (1997)

[35] H. Chiriac, M. Tibu, V. Dobrea, "Magnetic properties of amorphous wires with different diameters", Journal of Magnetism and Magnetic Materials 290-291 1142-1145 (2005)

References

_____

[36] Giselher Herzer, "Magnetic materials for electronic article surveillance", Journal of Magnetism and Magnetic Materials 254-255 598-602 (2003)

[37] H.L. Seet, S.H. See, X.P. Li, J.Y. Lee, K.Y.T. Lee, S.H. Teoh, C.T. Lim, "Study of the parameters of electroplating of ferromagnetic materials in relation to material permeability" *Materials Science Forum* 437-438 475-478 (2003)

[38] S.H. See, H.L. Seet, X.P. Li, J.Y. Lee, K.Y.T. Lee, S.H. Teoh, C.T. Lim, "Effect of nanocrystalline electroplating of NiFe on the material permeability", Materials Science Forum 437-438 53-56 (2003)

[39] H.L. Seet, X.P. Li, K.S. lee, C.S. Yap, H.M. Zheng, "Development of micro $Ni_{80}Fe_{20}$/Cu composite wire by cold drawing" *Thin Solid Films* 505 148-151 (2006)

[40] H.L. Seet, X.P. Li, J.B. Yi, W.Y. Ooi, K.S. Lee, "Effect of deposition methods on the magnetic properties of nanocrystalline permalloy" *Journal of Alloys and Compounds* 449 284-287 (2008)

[41] X.P. Li, H.L. Seet, Z.J. Zhao, Y.K. Kong, "Development of high permeability nanocrystalline ferromagnetic materials by pulse plating", *Journal of Metastable and Nanocrystalline Materials* 23 163-166 (2005)

[42] X.P. Li, H.L. Seet, Z.J. Zhao, Y.K. Kong, H. Gong, "Nanocrystalline deposition for developing high permeability ferromagnetic materials", *Transactions of the Materials Research Society of Japan* 29(4) 1695-1700 (2004)

[43] J. Velleuer, A.G. Munoz, H. Yakabchuk, C. Schiefer, A. Hackl, E. Kisker, "Giant magneto impedance in electroplated NiFeMo/Cu microwires", *Journal of Magnetism and Magnetic Materials* 311 651-657 (2007)

References

---

[44] Taylor, W. P., Schneider, M., Baltes, H., & Allen, M. G., "Electroplated Soft Magnetic Materials for Microsensors and Microactuators" *1997 International Conference on Solid-state Sensors and Actuators, Chicago*, 1445-1448 (1997)

[45] Wikipedia The Free Encyclopedia. *Supermalloy.* Retrieved March 21, 2007, from http://en.wikipedia.org/wiki/Supermalloy

[46] Nie, H. B., Pakhomov, A. B., Yan, X., Zhang, X. X., & Knobel, M., "Giant magnetoimpedance in crystalline Mumetal", *Solid State Communications 112* 285-289 (1999)

[47] Magnet Sales & Service Limited. Cast Alcomax Magnets. Retrieved March 20, 2007, http://www.magnetsales.co.uk/magnets/castalcomax.html.

[48] Magnet Sales & Manufacturing Company, Inc. (2000). Alnico Magnets. Retrieved on March 21st 2007, http://www.magnetsales.com/Alnico/Al1.htm

[49] M. Knobel, M. Vazquez, L. Kraus, "Giant magnetoimpedance" *Handbook of Magnetic Materials* 15 497-563 (2003)

[50] A.S. Antonov, N.A. Buznikov, I.T. Iakubov, A.N. Lagarkov, A.L. Rakhmanov, "Nonlinear magnetization reversal of Co-based amorphous microwires induced by an ac current" Journal of Physics D: Applied Physics 34 752-757 (2001)

[51] G.V. Kurlyandskaya, E.Krisker, H. Yakabchuk, N.G. Bebenin, "Non-linear giant magnetoimpedance" Journal of Magnetism and Magnetic Material 240 206-208 (2002)

[52] Mordechay Schlesinger, Milan Paunovic, Modern Electroplating, John Wiley & Sons, Inc., New York (2000)

References
_____

[53] N.V. Parthasaradhy, Practical Electroplating Handbook, Prentice Hall, New Jersy (1989)

[54] Allen Bai and Chi-Chang Hu, "Compositional controlling of Co-Ni and Fe-Co alloys using pulse-reverse electroplating through means of experimental strategies," *Electrochimica Acta* 50 1335-1345 (2005)

[55] K.-M. Yin, S.-L. Jan, C.-C. Lee, "Current Pulse with Reverse Plating of Nickel-Iron Alloys in a Sulphate Bath," *Surface and Coatings Technology* 88 219-225 (1996)

[56] E. Beltowska-Lehman and A. Riesenkampf, "An Investigation of the Electrodeposition Kinetics of Permalloys Thin Films Using a Rotating Disc Electrode," *Surface Technology* 11 349-355 (1980)

[57] N.A. Buznilov, A.S. Antonov, ect. "Giant magnetoimpedance in composite wires with insulator layer between non-magnetic core and soft magnetic shell" J. Magn. Magn. Mater. 300 (2006) e63.

[58] N.A. Usov, A.S. Antonov, A.N. Lagar'kov, J. Magn. Magn. Mater. 185 (1998) 159.

[59] D.P. Makhnovskiy, L.V. Panina, D.J. Mapps, Phys. Rev. B 63 (2001) 144424.

[60] A. Gromov, V. Korenivski, J. Phys. D 33 (2000) 773.

[61] K. Mohri, T. Kohhzawa, K. Kawashima, H. Yoshida, L.V. Panina, IEEE Trans. Magn. 28 (1992) 3150.

[62] Z.M. Wu, Z.J. Zhao, L.P. Liu, et al., Sensors Actuators A 137 (2007) 244.

[63] L.P. Liu, Z.J. Zhao, J.C. Zhang, et al., J. Magn. Magn. Mater. 305 (2006) 212.

[64] Beddoes, J., Bibby, M. J. (1999). *Principles of Metal Manufacturing Processes*. London: Arnold.

[65] H.L. Seet, S.H. See, X.P. Li, J.Y. Lee, K.Y.T. Lee, S.H. Teoh, C.T. Lim, "Study of the parameters of electroplating of ferromagnetic materials in relation to material permeability" *Materials Science Forum* 437-438 475-478 (2003)